POWER TRANSFER BETWEEN NON-SINUSOIDAL SOURCE AND LOAD ACROSS IMPEDANCE NETWORK

By

Abdulrhman Alshaabani

A THESIS

Submitted to
Michigan State University
in partial fulfillment of the requirements
for the degree of

Electrical Engineering – Master of Science

2017

ABSTRACT

POWER TRANSFER BETWEEN NON-SINUSOIDAL SOURCE AND LOAD ACROSS IMPEDANCE NETWORK

By

Abdulrhman Alshaabani

Renewable energy sources are of immense interest as increasing their use is a potential method for climate change mitigation. Therefore, it is important to consider ways to improve the applications of renewable energies. In this thesis, the fundamentals of contactless power transformers are presented and discussed. The power transfer between a non-sinusoidal source and a non-sinusoidal load across an inductive network is a new model that can transfer different ranges of power without cables. The main advantage of this new model of transferring power is that the reluctance transformer value is included when it is applied with compensation capacitors. In this thesis, the calculation of the resonant compensated capacitors' values includes the whole value of self-inductance with its reluctance. The power transfer system is applied to the high-power wind electric energy system. Consequently, the efficiency of transferring a high level of power is improved by applying the compensation capacitors. The MATHCAD software is used for calculating the analytical equations while the power transfer system simulation is carried out by the SABER software.

ACKNOWLEDGEMENTS

I would like to convey my sincere gratitude to Dr. Bingsen Wang. This project would not have been possible without his continuous advice and assistance. Dr. Wang's patient guidance, constructive critiques, expansive knowledge, and superior research approach have been invaluable during this research process.

I would like to thank my committee members Dr. Fang Z. Peng and Dr. Joydeep Mitra for giving their valuable time to serve on my master's committee. Additionally, I would like to thank my lab mate Ameer Janabi, as well as Yaqub Mahnashi and Saleh Almasabi who have supported me in various ways.

Finally, I would like to thank my family for their constant support, understanding, and patience throughout the duration of my studies.

TABLE OF CONTENTS

LIST OF TABLES

LIST OF FIGURES

CHAPTER 1

INTRODUCTION

In the 19th century, Nikola Tesla was a pioneer in electrical engineering, and had innovative ideas to wirelessly transfer electrical power [1, 2]. Since that time, engineers have desired to wirelessly transfer electrical power via air.

It is well known that a small amount of electrical power with a very high frequency can be submitted wirelessly through the long distance of a radiation field. However, the first real effort to transfer high power with a frequency of around 3-kHz was by Hutin and Le-Blanc in 1894. This is useful for devices that need a high amount of power with certain frequencies or zero frequency such as the rechargeable electric vehicle battery, or different applications that need a different amount of frequency to power them. This attempt was made to recharge Electric vehicle (EV) battery [3]. After that time, many scientists and researchers sought to improve and control wireless power transfer which is known as the inductive power transfer (IPT) system. The IPT system uses electromagnetic induction which submits a high power from one external induction coil to a receiver inaction coil via air [4].

The IPT system as shown in Figure 1.1 has many advantages. This motivates many factories and researchers to make efforts to improve it. One of the main advantages of the IPT system is that it is safer than an electric station's electrical cord that plugs into an EV for a high power charging [4,5]. This safety feature works better when an EV is charged at home. The IPT system is safer to charge electric cars in the home than the cord method because the cord requires more power

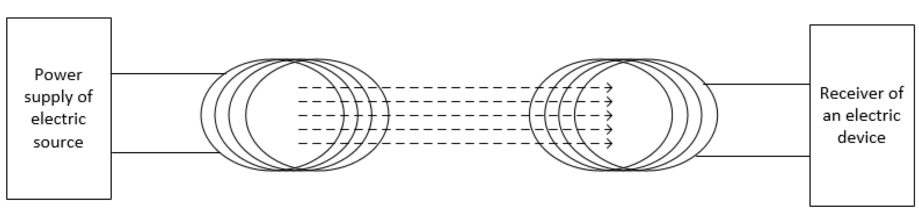

Figure 1.1 The basic idea of IPT system

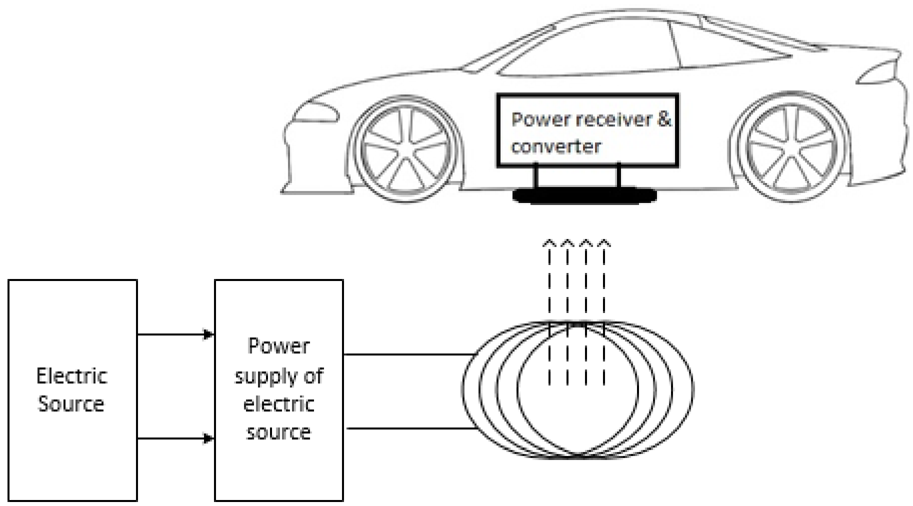

Figure 1.2 The electric charging station with IPT system

for delivery. Another advantage to using a contactless power transfer (CPT) system is avoidance of the use of a physical contact during harsh conditions weather such as rainy or snowy days. Additionally, the CPT system can circumvent some issues that happen in the winter season where a plug cord freezes [6]. Also, this technology reduces the maintenance operation that is required for a galvanic isolated connector and wiring, and the charging electric station's connectors. [7].

The IPT system can be used for EV and hybrid electric vehicles (HEV) in order to charge their batteries. This feature can enable the increased spread of EV and HEV technologies worldwide [6]. Therefore, this could lead to a reduction in the use of internal combustion engine (ICE) vehicles. ICE vehicles have many disadvantages that can negatively impact the environment such as causing exhaust emissions. These emissions effect the ozone layer and consequently human health [8, 9]. The IPT system can be applied in different ways in order to recharge the EV. One of the main ways to recharge an EV is by applying the IPT system to an electric station which is for EV charging. Figure 1.2 shows a design that uses the IPT system to charge an EV in an electric station rather than using conventional methods. Conventional methods include plugging the electric cord and connector to an EV. The IPT method can help senior citizens and people that are disabled to conveniently recharge their cars. Also, there are other benefits to this method besides what was previously mentioned. Some of these benefits include that this method has more reliability and recharges an EV faster and easier than conventional methods. Additionally, It is an extremely quiet process and has nearly invisible infrastructure [8]. Another way to recharge an EV battery through the IPT system application is called the roadway electrification as shown in Figure 1.3. The roadway electrification method works when an electric vehicle moves along a lane of an electric field section, then the EV will receive the electric power that is submitted by the electric field section [6]. This method can solve the main issue of EV which is the limitation of battery storage for the EV. Also, it can reduce the high price of an EV compared to ICE vehicles by decreasing battery storage requirement [6]. The roadway electrification method can be used inside cities for different purposes such as in South Korea. On the campus of Korea Advanced Institute of Science and Technology (KAIST) in South Korea the roadway electrification was applied to recharge buses while the buses ran [10]. Also, the other benefit to this method is saving time for recharging the EV battery. Moreover, the contactless power transformer can be used for several renewable energy sources. some energy sources such as solar and wind energies are using High frequency transformer [11–13]. For instance, the photovoltaic can be used as an extra assisting source in order to charge the electric vehicle [11]. The assisting photovoltaic source is taking the solar energy by solar cells and converting it to direct current. The inverter then converts the direct current to alternative current with high frequency. The amount of power with high frequency will pass through a high frequency transformer which is a type of solid state transformer. After that, a rectifier converts the alternative current with high frequency to direct current in order to feed the battery by direct current. In this case, the high transformer can be replaced by the inductive power transfer. In addition, another major renewable source that can be used with the inductive power transfer is the wind electric energy system. A majority of researches focus on the topology of off shore wind turbines [12, 13]. Also, most of these topologies have high frequency transformer. The high frequency transformer is used in order to reduce the equipments sizes, hence the weight and cost of the system are reduced. Therefore, the inductive power transfer possesses advantages over the high frequency transformer in the wind electric energy system. Another feature of applying

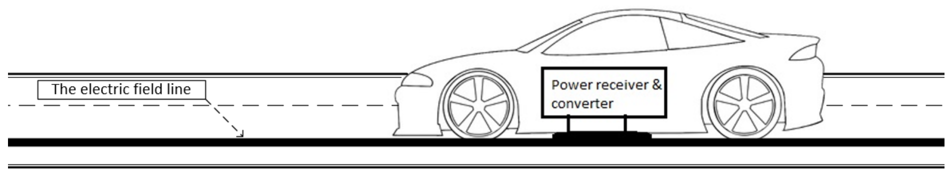

Figure 1.3 The roadway electrification method with IPT system

inductive power transfer beside reducing the size equipments is transferring the high amount of power without the need for cables. This will solve many problems that happens for maintenance operation. Also, it can work as insulation instead of galvanic isolation which helps to protect the wind electric system.

1.1 Motivation

There has been an increase in the amount of research being conducted to improve inductive power transfer methods and efficiencies. The aim is to use findings of this research in different applications [14]. Inductive power transfer can be used to wirelessly charge a battery [1,9,14]. The electric vehicle battery charger is one of the main applications for contactless power transfer. The IPT system can be used to transfer different amounts of power from various renewable energy sources. A high amount of energy can be applied to a wind electric energy system via a contactless power transfer system. Additionally, this power transfer method is implemented in the medical field for biomedical implant devices [2, 9]. Different power ranges are used based on the requirements of the device.

1.2 Objective

Many publications focus on improving the efficiency and control of inductive power transfer (IPT). However, most of the research uses a similar model of IPT. This model is used regardless of the transformer's reluctance and how it can affect the power transfer's efficiency. The reluctance effects the efficiency when the distance of the air gap between the transformer's two circuit sides increases. Thus, in this thesis, the new model of power transfer system solves this issue by applying a specific transformer model. This model includes transformer reluctance when the coefficient of magnetic coupling is changing. Moreover, this model of power transfer can transfer electric power between a non-sinusoidal source and a non-sinusoidal load over an impedance network.

1.3 Organization of the thesis

The content of this thesis is divided into five chapters, which are summarized in the following:

In order to build a good knowledge about the new model of wireless power transfer system, chapter 2 begins with an analysis of a specific equivalent circuit transformer model. This transformer model will be applied to the power transfer system. Therefore, the output results of this model are shown in the end of this chapter. Moreover, the efficiency of this power transfer model between a non-sinusoidal source and a non-sinusoidal load across an impedance network is calculated.

After showing the basic principle analysis of the new power transfer system, the resonant compensation calculation is presented in chapter 3. Additionally, the efficiency limitations of resonant compensation are shown later in this chapter.

The power transfer system between a non-sinusoidal source and a non-sinusoidal load is applied to the wind electric energy system as an application in chapter 4. Moreover, a series-series resonant circuit are applied with the power transfer system in wind electric energy system in order to improve the efficiency.

Based on the results of all previous chapters for the power transfer system between a non-sinusoidal source and a non-sinusoidal load across an impedance network, the conclusion is presented in chapter 5. Future work suggestions are also discussed for this model; from optimization advancements to its application in the world.

CHAPTER 2

FUNDAMENTAL OF A POWER TRANSFER SYSTEM BETWEEN NON-SINUSOIDAL SOURCE AND LOAD

This chapter begins with an analysis of a transformer's equivalent circuit and the principle advantages of the analytical transformer equations to introduce the new model of power transfer converter with a high frequency transformer between non-sinusoidal source and load. The structure for power transfer system is shown as a block diagram in Figure 2.1. In section 1.2, the basic functionality of a power transfer system between non-sinusoidal source and load are described and applied on SABER and MATHCAD software. In section 1.3, conclusion of the power transfer system between non-sinusoidal source and load across an impedance network are discussed based on the results of software's outputs.

2.1 Transformer equivalent circuit

2.1.1 Analysis of equivalent circuit

For a deep understanding of power transfer between a non-sinusoidal source and a non-sinusoidal load across an impedance network, analysis of a transformer modeling of two winding coupled

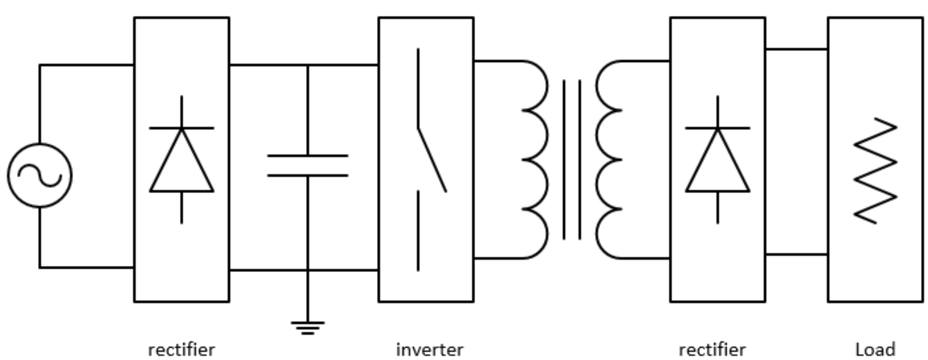

Figure 2.1 Block diagram of power transfer system with high frequency transformer

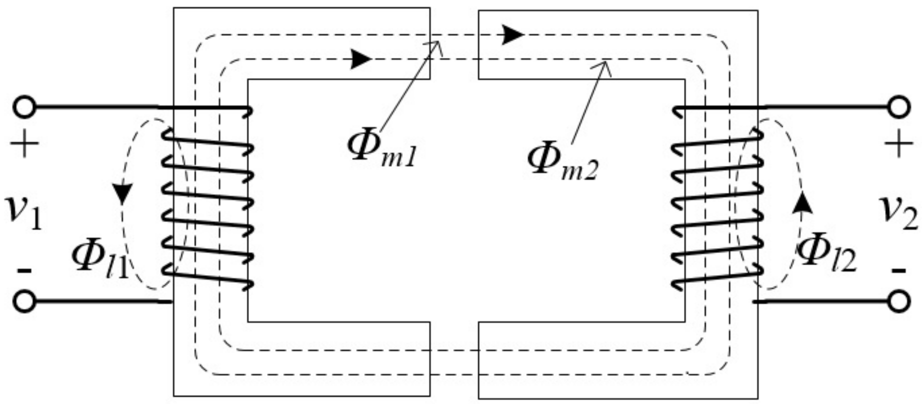

Figure 2.2 The coupled inductors.

inductors inside the system is explained in this section. The coupled inductors are shown in Figure 2.2 that consists of two windings on the magnetic core. The turn number of each windings is N_1 and N_2. The mutual flux is a flux that links both windings whereas the leakage flux is a flux that links with one winding [15].

Where Φ_{m1} is the magnetizing flux of primary coil of the transformer that will be proportional to the entered current of primary coil i_1 and number of its turns N_1. $(N_1 i_1)$ is the magnetomotive force. R_m is a magnetic reluctance of the core that Φ_{m1} is inversely proportional to the magnetic reluctance.

$$\Phi_{m1} = \frac{N_1 i_1}{R_m} \tag{2.1}$$

$$R_m = \frac{L}{A\mu} \tag{2.2}$$

Where L is the length of transformer core and the air gap of contactless transformer. μ is the permeability of the material. A is the cross-section of transformer core.

$$\Phi_{L1} = \frac{N_1 i_1}{R_{l1}} \tag{2.3}$$

Φ_{l1} is the leakage flux of primary coil which is proportional to the magnetomotive force. R_{l1} is the leakage resistance.

$$\Phi_{m2} = \frac{N_2 i_2}{R_m} \tag{2.4}$$

Where Φ_{m2} is the magnetizing flux of secondary coil of the transformer.

$$\Phi_{L2} = \frac{N_2 i_2}{R_{l2}} \tag{2.5}$$

Φ_{l2} is the leakage flux of secondary coil. R_{l2} is the leakage resistance of secondary coil. To derive the voltage formulas for both sides, the previous equations will be used as following

$$v_1 = N_1 * \frac{d}{dt}(\Phi_{m1} + \Phi_{L1} + \Phi_{m2}) \tag{2.6}$$

$$v_2 = N_2 * \frac{d}{dt}(\Phi_{m1} + \Phi_{L2} + \Phi_{m2}) \tag{2.7}$$

Now, equations 2.1-2.5 can be inserted in to equations 2.6 and 2.7

$$v_1 = N_1 * \frac{d}{dt}(\frac{N_1 i_1}{R_m} + \frac{N_1 i_1}{R_L 1} + \frac{N_2 i_2}{R_m}) \tag{2.8}$$

$$v_2 = N_2 * \frac{d}{dt}(\frac{N_1 i_1}{R_m} + \frac{N_2 i_2}{R_{L2}} + \frac{N_2 i_2}{R_m}) \tag{2.9}$$

So, the leakage inductance of primary coil is

$$L_{L1} = \frac{N_1^2}{R_{L1}} \tag{2.10}$$

The magnetizing inductance of primary coil

$$L_{m1} = \frac{N_1^2}{R_m} \tag{2.11}$$

The leakage inductance of secondary coil is

$$L_{L2} = \frac{N_2^2}{R_{L2}} \tag{2.12}$$

The magnetizing inductance of secondary coil

$$L_{m2} = \frac{N_2^2}{R_m} \tag{2.13}$$

The mutual inductance of transformer L_{12}

$$L_{12} = \frac{N_1 N_2}{R_m} \tag{2.14}$$

The voltage formulas of both sides can be expressed as follows

$$v_1 = (L_{L1} + L_{m1})\frac{di_1}{dt} + L_{12}\frac{di_2}{dt} \tag{2.15}$$

$$v_2 = (L_{L2} + L_{m2})\frac{di_2}{dt} + L_{12}\frac{di_1}{dt} \tag{2.16}$$

Where (L_{l1}+L_{m1}) is the self-inductance of primary coil which can be called L_1. Also, (L_{l2}+L_{m2}) is the self-inductance of secondary coil which is L_2 .

$$v_1 = L_1\frac{di_1}{dt} + L_{12}\frac{di_2}{dt} \tag{2.17}$$

$$v_2 = L_2\frac{di_2}{dt} + L_{12}\frac{di_1}{dt} \tag{2.18}$$

The mutual inductance of transformer L_{12} can be called L_M for more simplified. Then the classical equations for the two windings coupled circuit are

$$v_1 = L_1\frac{di_1}{dt} + L_M\frac{di_2}{dt} \tag{2.19}$$

$$v_2 = L_2\frac{di_2}{dt} + L_M\frac{di_1}{dt} \tag{2.20}$$

The coefficient of magnetic coupling k is explained in [15, 16] as coupling coefficient between two magnetic circuits that is defined as

$$k = \frac{L_M}{\sqrt{L_1 L_2}} \tag{2.21}$$

Based on 2.19 the equivalent circuit can be rewritten as the following when the secondary side refers to the primary side

$$v_1 = L_1\frac{di_1}{dt} + NL_M\frac{d}{dt}(\frac{i_2}{N}) \tag{2.22}$$

$$Nv_2 = N^2 L_2\frac{d}{dt}(\frac{i_2}{N}) + NL_M\frac{di_1}{dt} \tag{2.23}$$

The ratio of turns number N can be chosen as $N = \sqrt{\frac{L_1}{L_2}}$ as explained in [16].

$$N = \sqrt{\frac{L_1}{L_2}} \tag{2.24}$$

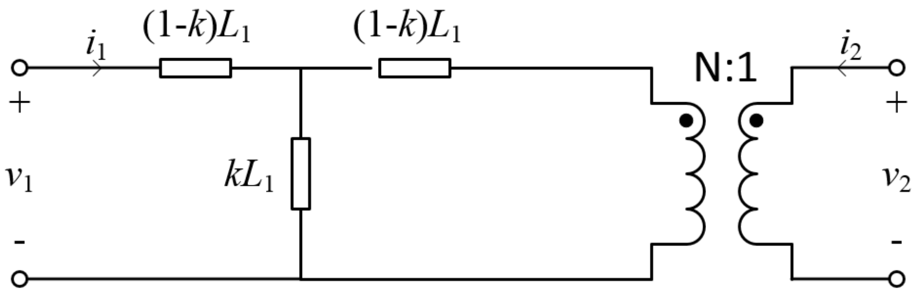

Figure 2.3 The equivalent circuit corresponded when $N = \sqrt{\frac{L_1}{L_2}}$

Substitude 2.24 to 2.22 and 2.23

$$v_1 = L_1 \frac{di_1}{dt} + (\sqrt{\frac{L_1}{L_2}}) L_M \frac{d}{dt} (\frac{i_2}{(\sqrt{\frac{L_1}{L_2}})}) \tag{2.25}$$

$$(\sqrt{\frac{L_1}{L_2}}) v_2 = (\sqrt{\frac{L_1}{L_2}})^2 L_2 \frac{d}{dt} (\frac{i_2}{(\sqrt{\frac{L_1}{L_2}})}) + (\sqrt{\frac{L_1}{L_2}}) L_M \frac{di_1}{dt} \tag{2.26}$$

Then the equivalent circuit corresponded is shown in Figure 2.3

2.2 Basic operation of contactless converter

After the circuit of equivalent transformer has been analyzed, the basic functionality of the PT system between non-sinusoidal source and load is introduced in this section. Figure 2.4 shows the full topology of this model. All components of the system are assumed as ideal components and without losses during the derivation.

The full-bridge inverter, which is on the primary side of the PT system, is operated with 50% duty cycle. The transformer output voltage terminal v_2 follows the same polarity sign as the inverter output voltage terminal at the same interval. When the magnetic coupling coefficient is high, a magnetizing inductance becomes high L_μ. While the magnetizing inductance is large, the primary and secondary inductances of the transformer is small. Hence, the magnetizing current value

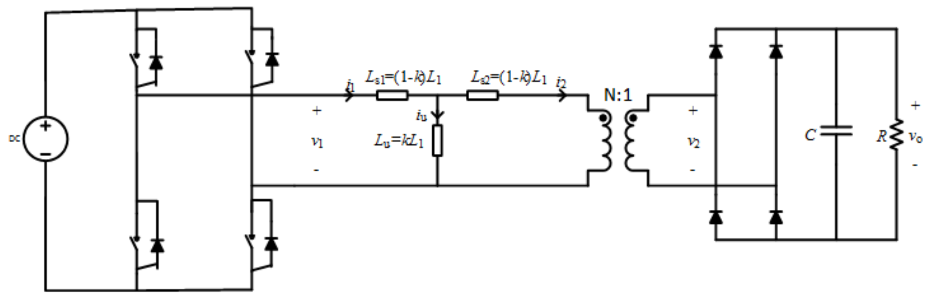

Figure 2.4 The power transfer between a non-sinusoidal source and a non-sinusoidal load across the impedance network model.

Table 2.1 Parameters of the power transfer model.

Parameter	Variable	Value
Output power	P_{out}	$\leq$5k W
Input DC voltage	V_1	400 V
Output DC voltage	V_{out}	$\leq$400 V
Switching frequency	f_{sw}	10k Hz
Primary self-inductance	L_1	3m H
Secondary self-inductance	L_2	3m H

i_μ is so small while the primary and secondary currents are almost the same and have a larger value compared with i_μ. Therefore, the magnetizing current can be neglected for the following calculation. Figure 2.5 shows the effects of magnetic coupling of the contactless transformer when the air gap distance between primary and secondary sides begins larger with $k = 0.98$ and $k = 0.96$. It is noticeable that the voltage value of $v_2(t)$ is affected by increasing the air gap between the two sides of transformer. Additionally, the average current values of both $i_1(t)$ and $i_2(t)$ are inversely proportional with the distance between the sides of contactless transformer. However, the secondary side of the converter consists of a passive diode rectifier and output capacitor. Then the zero-crossing instants of the voltage $v_2(t)$ and $i_2(t)$ have to be in phase based on the constraints of the passive diode rectifier, i.e. $v_2(t)$ and $i_2(t)$ cross the zero time axis at the same time [17]. However, the parameter values, which are used in this power transfer system model, are shown in the Table 2.1 [9].

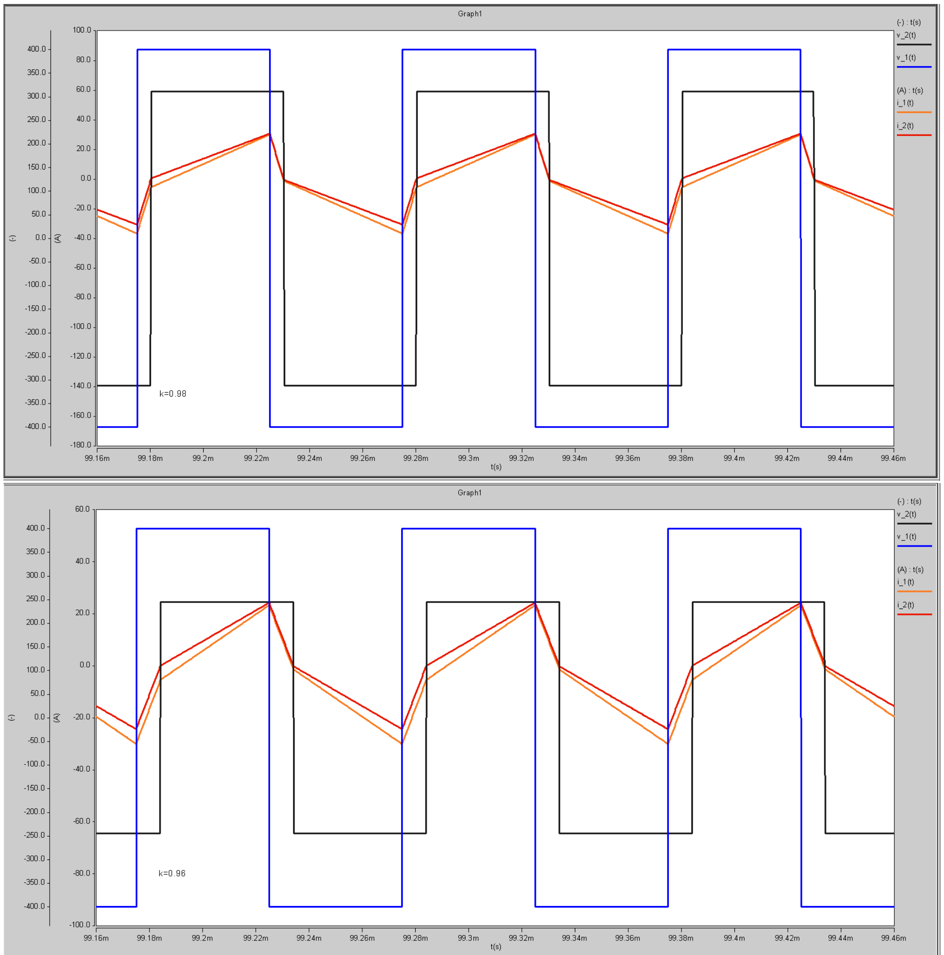

Figure 2.5 The $v_1(t), v_2(t), i_1(t)$, and $i_2(t)$ are shown when the magnetic coupling coefficient $k = 0.98$, as in the top figure, and $k = 0.96$ in the down figure.

2.3 Fundamental equations of the converter

After showing the basic operations of the PT system between a non-sinusoidal source and a non-sinusoidal load, the fundamental equations of this converter are represented in this section. The instantaneous output voltage of the inverter $v_1(t)$ as shown in Figure 2.5 can be expressed as following equation:

$$v_{1(n)}(t) = \sum_{n=1}^{\infty} \frac{4 * V_{DC}}{n\pi} \sin(n\omega t) \tag{2.27}$$

where n=1,3,5... and ω is the angular frequency which is $\omega = 2 * \pi * f_{sw}$. The switching frequency f_{sw} is the frequency over one cycle that is applied on the switches of inverter. However, another important formula that should be mentioned is the amplitude spectrum voltage. The amplitude spectrum of the inverter output voltage $v_1(t)$ is, as shown bellow, introduced the amplitude value of each harmonics of $v_1(t)$.

$$\hat{V}_{1(n)} = \frac{4 * V_{DC}}{n\pi} \tag{2.28}$$

The input voltage of the rectifier on secondary side of the converter can be represented as related to the voltage ratio k_{12} as following equation

$$v_{2(n)}(t) = k_{12} * \sum_{n=1}^{\infty} \frac{4 * V_{DC}}{n\pi} \sin(n\omega t + \delta) \tag{2.29}$$

where δ is the phase angle difference between $v_1(t)$ and $v_2(t)$.
δ can be calculated by a new method that unpublished work by Dr. Bingsen Wang as shown below.

$$\delta = \frac{\pi}{2}(1 - k_{21}) \tag{2.30}$$

Equation 2.30 shows the relationship between the voltage ratio k_{21} and the phase angle difference. However, in order to find the voltage ratio k_{12} formula between $v_{1(n)}(t)$ and $v_{2(n)}(t)$ of the non-sinusoidal waveforms, Dr. Bingsen Wang method is applied.
Thevenin's theorem is applied to the PT converter topology, which is shown in Figure 2.4, for simplified the calculation to find the voltage ratio. In Figure 2.6 is shown that the PT model after applying Thevenin's theorem. Also, the inductors resistances can be ignored while the resistances are very small. So, the relationship between $v_{1(n)}$ and the thevenin voltage which can be represented as $v_{th(n)}(k)$ is

$$v_{th(n)}(k) = v_{1(n)} \frac{L_\mu}{L_{s1} + L_\mu} \tag{2.31}$$

Also, the inductors can be combined by thevenin theorem as follows

$$n\omega L_{th} = n\omega(\frac{L_{s1}L_\mu}{L_{s1} + L_\mu} + L_{s2}) \tag{2.32}$$

where L_{th} represents the thevenin inductance.

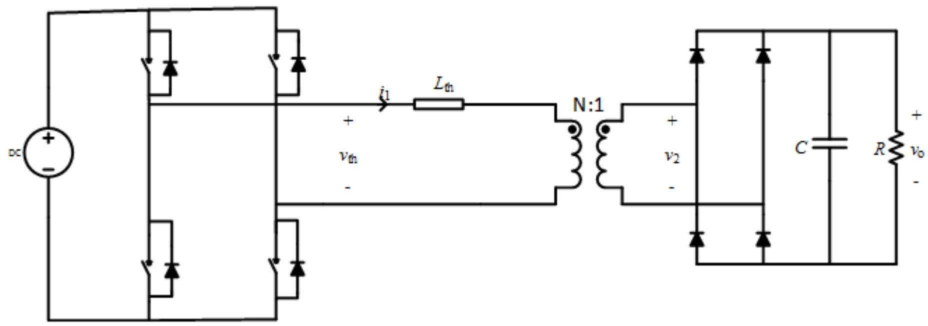

Figure 2.6 The power transfer model after applying Thevenin theorem.

Hence, the average value of input power that is drawn from the source is

$$P = \frac{2}{T_s}\int_0^{\frac{T_s}{2}} v_{th}(t)i(t)dt \tag{2.33}$$

$$P = P_1 + P_2 \tag{2.34}$$

with

$$P_1 = \frac{2}{T_s}\int_0^{\frac{\delta}{\omega}} V_{th}(k)(-I + \frac{V_{th}(k)+V_2}{L_{th}}t)dt \tag{2.35}$$

$$P_2 = \frac{2}{T_s}\int_{\frac{\delta}{\omega}}^{\frac{T_s}{2}} V_{th}(k)((-I + \frac{V_{th}(k)+V_2}{L_{th}}\frac{\delta}{\omega}) + \frac{V_{th}(k)-V_2}{L_{th}}(t-\frac{\delta}{\omega}))dt \tag{2.36}$$

$$P = \frac{\delta}{\pi}V_{th}(k)[0.5\frac{\pi(V_{th}(k)+V_2)}{\omega L_{th}} - I] \tag{2.37}$$

So, the current continuity at $t = \frac{\delta}{\omega}$ is

$$-I + \frac{V_{th}(k)+V_2}{\omega L_{th}}\delta = I - \frac{V_{th}(k)-V_2}{\omega L_{th}}(\pi-\delta) \tag{2.38}$$

$$I = \frac{1}{\omega L_{th}}[\frac{\pi}{2}(V_{th}(k)-V_2) + V_2\delta] \tag{2.39}$$

Equation 2.39 can be inserted to equation 2.37 to have following formula

$$P = \frac{V_{th}(k)V_2}{\omega L_{th}}(1-\frac{\delta}{\pi})\delta \tag{2.40}$$

Hence, the voltage ratio $k_{2th}(k) = \frac{V_2}{V_{th}(k)}$ can be determine based on the power balance as following

$$\frac{V_{th}(k)V_2}{\omega L_{th}}\frac{\delta(\pi-\delta)}{\pi} = \frac{V_2^2}{R_{Load}} \tag{2.41}$$

$$\frac{\delta(\pi-\delta)}{\pi} = \frac{\omega L_{th}}{R_{Load}} k_{2th}(k) \tag{2.42}$$

Substituting equation 2.30 into equation 2.42 yields

$$k_{2th}(k) = \frac{2}{\pi}[\sqrt{(\frac{\omega L_{th}}{R_{Load}})^2 + (\frac{\pi}{2})^2} - \frac{\omega L_{th}}{R_{Load}}] \tag{2.43}$$

To determine the voltage ratio $k_{21} = \frac{V_2}{V_1}$, can be found as following

$$k_{2th}(k) = \frac{V_2}{V_{th}(k)} = \frac{V_2}{V_1 \frac{L\mu}{L_{s1}+L\mu}} \tag{2.44}$$

So, the voltage ratio k_{21} is

$$k_{21}(k) = \frac{L\mu}{L_{s1}+L\mu} k_{2th}(k) \tag{2.45}$$

However, the voltage gain of the PT system can be found by the following equation 2.47. $V_{out}(k)$ is RMS value of the secondary voltage $v_{2(n)}(t)$that is applied on the rectifier.

$$V_{out}(k) = \sqrt{\frac{1}{T}\int_0^T (k_{12}(k) * \sum_{n=1}^{\infty} \frac{4 * V_{DC}}{n\pi} \sin(n\omega t + \delta))^2 dt} \tag{2.46}$$

$$gain(k) = \frac{V_{out}(k)}{V_1} \tag{2.47}$$

Where the voltage gain depends on the magnetic coupling coefficient k. In Figure 2.7 is shown that the related curve between the voltage gain and k where the voltage gain is increased whereas the distance of air gap is decreased. Therefore, the highest voltage gain ,which is with approximately unity value of the magnetic coupling coefficient k, is around $0.997 \approx 1$.

In order to determine the efficiency of the PT between a non-sinusoidal source and a non-sinusoidal load, the output and input power of this converter should be calculated as following

$$I_{in(n)}(k) = \frac{V_{th(n)}(k)}{Z_{th}(k)} \tag{2.48}$$

$I_{in(n)}(k)$ is the phaser form of input current by using Norton theorem. $Z_{th}(k)$ is the thevinin impedance of contactless transformer model.

$$Z_{th}(k) = jn\omega L_{th} \tag{2.49}$$

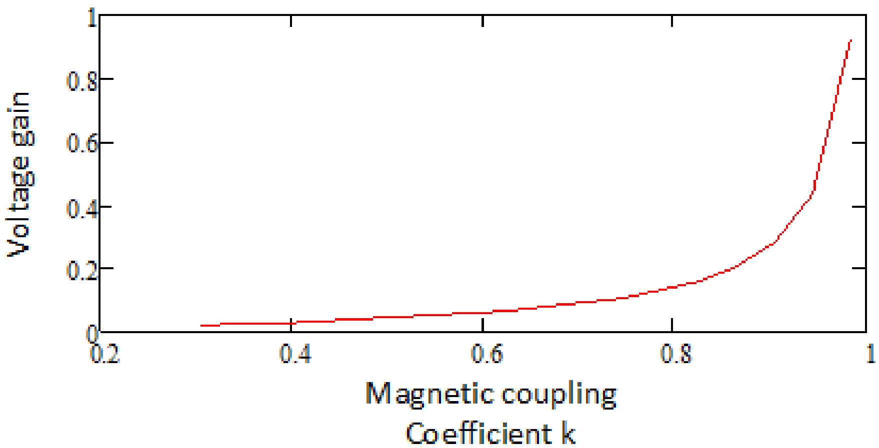

Figure 2.7 The voltage gain of power transfer between a non-sinusoidal and a non-sinusoidal load.

The instantaneous input current can be determine as following

$$i_{in}(k,t) = \sum_{n=1}^{\infty} |I_{in(n)}(k)| \sin(n\omega t + arg(I_{in(n)}(k))) \tag{2.50}$$

So, the average value of input power of PT between non-sinusoidal source and load can be determined as next equation

$$P_{in}(k) = \sum_{n=1}^{\infty} \frac{|I_{in(n)}(k)||V_{th(n)}(k)\frac{L_{s1}+L_\mu}{L_\mu}|}{2} \cos(arg(V_{th(n)}(k)\frac{L_{s1}+L_\mu}{L_\mu} - arg(I_{in(n)}(k))) \tag{2.51}$$

Based on the fact of rectifier which is the power balance, the input and output power of the rectifier should be equal [17].

$$\frac{1}{T}\int_0^T i_{in}(k,t)v_{2(n)}(k,t)dt = \frac{V_{out}(k)^2}{R_{Load}} \tag{2.52}$$

Then the average value of output power can be determined as following

$$P_{out} = \frac{1}{T}\int_0^T i_{in}(k,t)v_{2(n)}(k,t)dt \tag{2.53}$$

$$P_{out}(k) = \sum_{n=1}^{\infty} \frac{|I_{in(n)}(k)||V_{2(n)}(k)|}{2} \cos(arg(V_{2(n)}(k)) - arg(I_{in(n)}(k))) \tag{2.54}$$

The efficiency formula of this type of converter is shown next.

$$\eta(k) = \frac{P_{out}(k)}{P_{in}(k)} \tag{2.55}$$

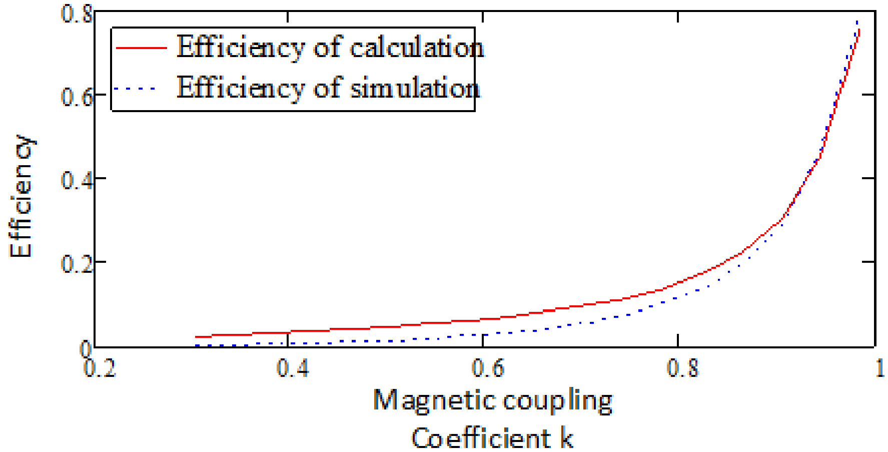

Figure 2.8 The efficiency curves of the power transfer system between a non-sinusoidal source and a non-sinusoidal load across the impedance network

2.3.1 The Efficiency Limitation

In the following, the limitation of the PT between a non-sinusoidal source and a non-sinusoidal load efficiency are shown in Figure 2.8. These curves were calculated with varies magnetic coupling coefficient k that is between 0.305 and 0.985 in order to find the lowest and better magnetic coupling coefficient k that can applied for this converter. The MATHCAD and SABER software were applied to find these curves.

Different magnetic coupling coefficient k can be taken arbitrarily to measure the efficiency of the converter and choose the lowest k with better efficiency. The magnetic coupling coefficient k that are chosen, are $k_1 = 0.99$,$k_2 = 0.98$,$k_3 = 0.97$, and $k_4 = 0.96$. So, the efficiency of each k values ,which were chosen, are as following

$$\eta(k_1) = \frac{P_{out}(k_1)}{P_{in}(k_1)} = 81.9\% \tag{2.56}$$

$$\eta(k_2) = \frac{P_{out}(k_2)}{P_{in}(k_2)} = 70.1\% \tag{2.57}$$

$$\eta(k_3) = \frac{P_{out}(k_3)}{P_{in}(k_3)} = 61\% \tag{2.58}$$

$$\eta(k_4) = \frac{P_{out}(k_4)}{P_{in}(k_4)} = 53.8\% \tag{2.59}$$

Hence, the PT system efficiency is decreased by increasing the air gap distance between the two contactless transformer sides. So, the lowest magnetic coupling coefficient k with efficiency that higher than 50% is $k = 0.96$ for this particular circuit.

2.4 Conclusion and Discussion

One of the main goals is to achieve a new model for a wireless power transfer system between a non-sinusoidal source and a non-sinusoidal load that can be calculated and adjusted more easily. This model, which is proposed in the beginning of this chapter, for power transfer conversion between a non-sinusoidal source and a non-sinusoidal load can be achieved by adjusting one value for both inductors. The main advantage of this model is that it simplifies dealing with this type of circuit by calculating one value for both primary and secondary coils of the contactless transformer. Another advantage of this model is the relationship between the voltage gain and the magnetic coupling coefficient k where the voltage gain can be determined as the desired value by adjusting the value of the magnetic coupling coefficient k. Additionally, the efficiency of the PT system has a direct relationship with the magnetic coupling coefficient k, where the efficiency increases with the increase of the value of k. However, the lowest value of k for efficiency more than 50% is 0.96. Hence, the resonance compensated capacitors will be applied on this model in the next chapter with the intention of achieving a better efficiency for the same value of k.

CHAPTER 3

THE RESONANT COMPENSATION OF POWER TRANSFER SYSTEM BETWEEN A NON-SINUSOIDAL SOURCE AND A NON-SINUSOIDAL LOAD

In this chapter, the resonant compensated capacitors are applied on the power transfer between a non-sinusoidal source and a non-sinusoidal load model as shown in Figure 3.1. Also, the fundamental frequency modeling is explained in section 3.1. In section 3.2, the effects of the resonant compensated capacitors on the efficiency limitation are represented for PT between a non-sinusoidal source and a non-sinusoidal load. In section 3.3, the resonant compensated capacitors which are applied on the power transfer system between non-sinusoidal source and load across an impedance network are discussed based on the results of software's outputs.

3.1 Modeled the fundamental frequency of the power transfer converter

Applying the resonant compensation capacitors in series with primary and secondary sides of the contactless transformer will help to reduce the effects of leakage inductances in this converter. Figure 3.2 shows the converter topology of power transfer between a non-sinusoidal source and a non-sinusoidal load model with the resonant compensation capacitors. The capacitors value C_1 and C_2 can be selected as the following equation.

$$f_{sw} = \frac{1}{2\pi\sqrt{L_{s1}C_1}} = \frac{1}{2\pi\sqrt{L_{s2}C_2}} \tag{3.1}$$

L_{s1} and L_{s2} are the primary and secondary self inductances multiplied by σ, respectively. where, $\sigma = (1-k)$ and k is the magnetic coupling coefficient.

The primary and secondary capacitors C_1 and C_2 are selected with the resonant frequency f_o where the resonant frequency is assumed to be equal to the switching frequency. So, both the capacitors become the resonant compensated capacitors for PT converter. In this situation, the secondary DC link voltage becomes a constant. This phenomena happens because the voltage across both leakage inductances L_{s1} and L_{s2} is canceled out by the voltage across both resonant capacitors

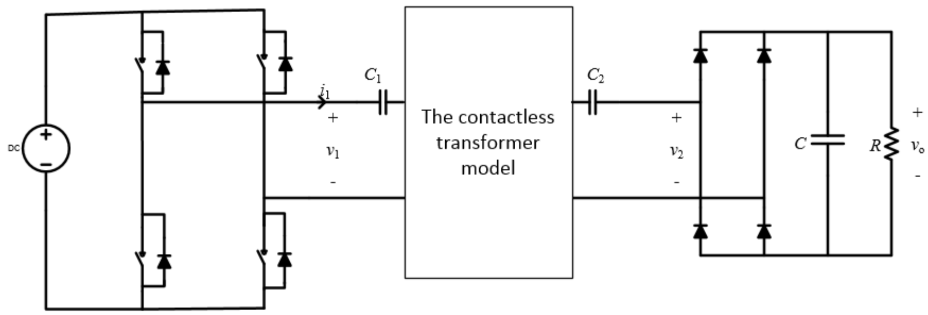

Figure 3.1 The power transfer between a non-sinusoidal source and a non-sinusoidal load across the impedance network with resonant compensation capacitors.

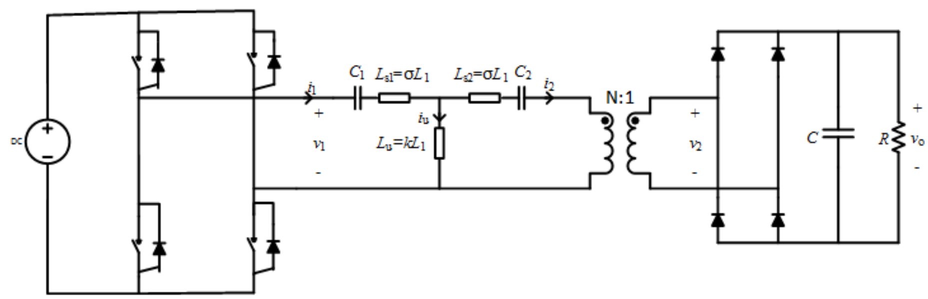

Figure 3.2 The series resonant compensation capacitors applied on the power transfer converter model.

C_1 and C_2. In Figure 3.3 it shows the output characteristic waveforms of the PT converter when $k = 0.98$. Additionally, the secondary voltage is a constant when the magnetic coupling coefficient k is changed as shown in Figure 3.4.

As shown in Figure 3.3, the resonant has the effect on the PT converter where it is filtering the higher harmonic voltage. Therefore, the current will have a sine wave shape that shows at the input to the resonant network where the input voltage that is applied to the circuit is a square wave. Because of this reason, the classical AC analysis techniques can be used for simplifying this circuit as explained in [18]. However, in order to determine the equivalent load resistance, the fundamental component of the square wave voltage $v_{1(1)}$ is applied to the resonant circuit. Hence, the voltage and current will have the sine waveform shape.

The fundamental of square wave voltage, which is applied to rectifier, is

$$v_{2(1)}(t) = \frac{4V_M}{(1)\pi}\cos((1)\omega t - \frac{\pi}{2}) \tag{3.2}$$

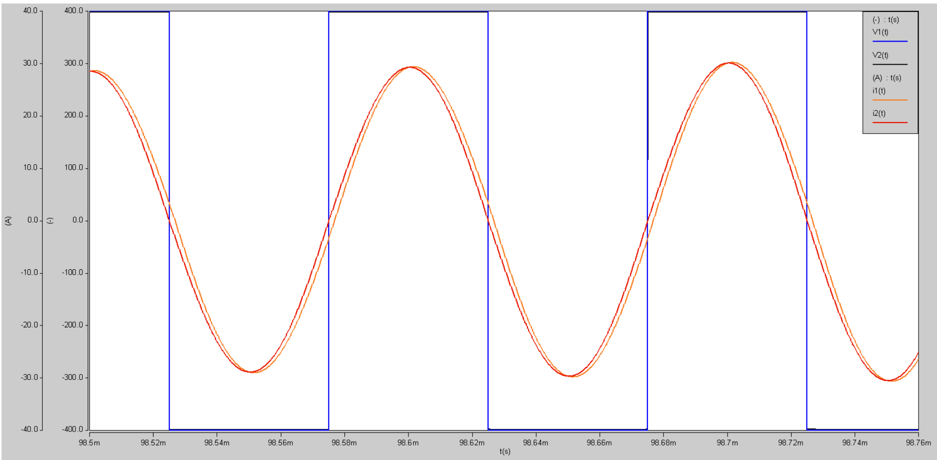

Figure 3.3 The output characteristics waveforms of the power transfer system when the magnetic coupling coefficient value is $k = 0.98$

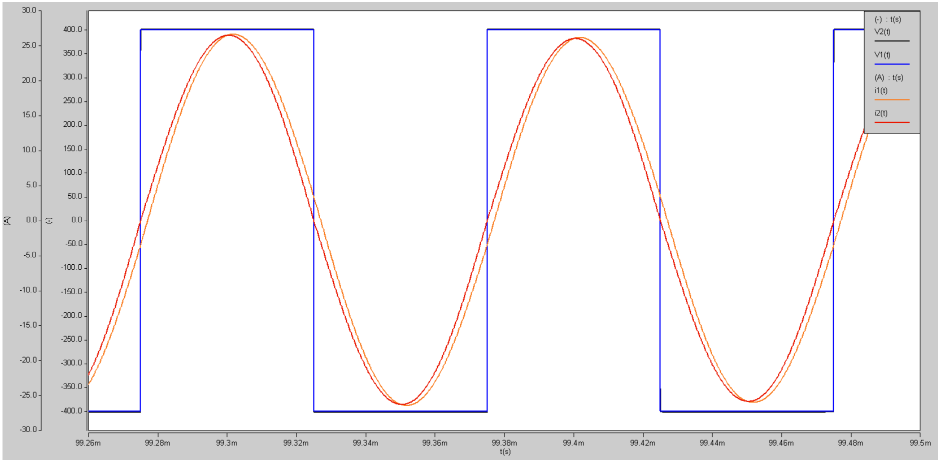

Figure 3.4 The output characteristics waveforms of the power transfer system when the magnetic coupling coefficient value is $k = 0.96$

$$V_{RMS} = \sqrt{\frac{1}{T}\int_0^T (v_{2(1)})^2 dt} \tag{3.3}$$

where $T = \frac{2\pi}{\omega}$ Then, the final derivation is

$$V_{RMS} = \frac{2V_{dc}\sqrt{2}}{(1)\pi} \tag{3.4}$$

While the current is a sine wave, then the average output current is [17]

$$I_{dc(out)} = \frac{2I_M}{\pi} \tag{3.5}$$

where the maximum current can be determine as

$$I_M = \frac{\pi I_{dc(out)}}{2} \tag{3.6}$$

where the RMS value of sine wave is

$$I_{RMS} = \frac{I_M}{\sqrt{2}} \tag{3.7}$$

So, the equivalent RMS voltage to output voltage is

$$I_{RMS} = \frac{\pi I_{dc(out)}}{2\sqrt{2}} \tag{3.8}$$

Then, the equivalent load resistance will be as

$$R_{eq,L} = \frac{V_{RMS}}{I_{RMS}} = \frac{8}{\pi^2} R_{Load} \tag{3.9}$$

In Figure 3.5 is shown the PT converter with the equivalent load resistance. Thevinin's theorem is applied to the PT converter with compensation capacitors for more simplifying as shown in Figure 3.6. The output voltage, which is applied on the equivalent load resistance, can be found as following

$$v_{out} = v_{1(1)} \frac{1}{1 + \frac{Z_{Th}}{R_{eq,L}}} \tag{3.10}$$

Where Z_{Th} represents the thevinin impedance of the resonant network.

$$Z_{s1} = j(\omega L_{s1} - \frac{1}{\omega C_1}) \tag{3.11}$$

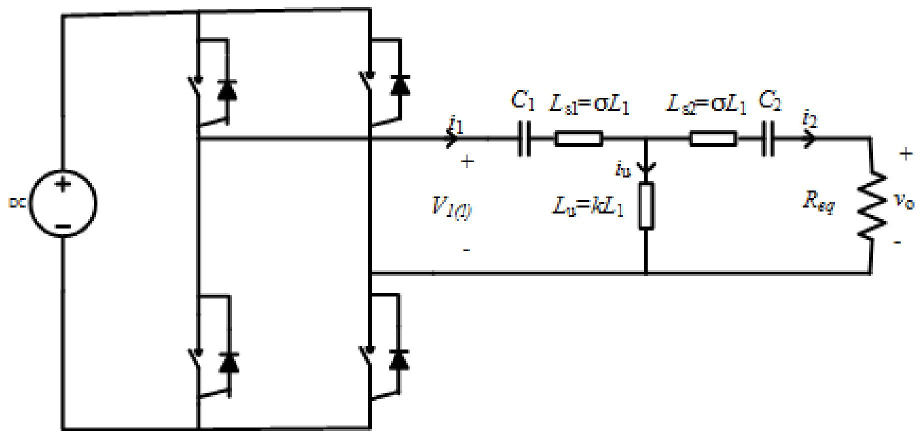

Figure 3.5 The full bridge rectifier with load resistance are replaced by the equivalent load resistance in the power transfer converter.

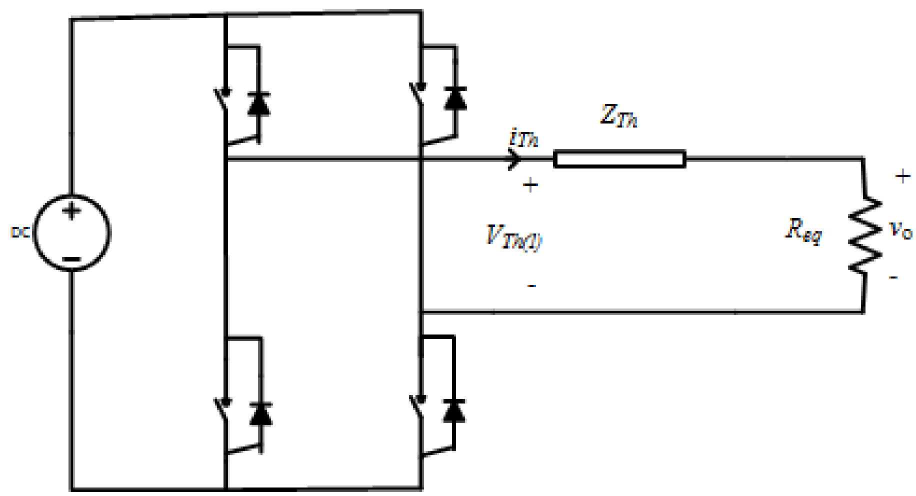

Figure 3.6 The thevinin voltage and impedance are applied on the power transfer converter with equivalent load resistance.

$$Z_{s2} = j(\omega L_{s2} - \frac{1}{\omega C_2}) \tag{3.12}$$

$$Z_{\mu} = j\omega L_{\mu} \tag{3.13}$$

Then Z_{Th} formula is shown below

$$Z_{Th} = (Z_{s1}//Z_{\mu}) + Z_{s2} \tag{3.14}$$

3.2 The efficiency limitation of power transfer system with compensation capacitors

In order to improve the power transfer system efficiency, the compensated capacitors are applied on the PT system as shown in Figure 3.7. This topology of power transfer between a non-sinusoidal source and a non-sinusoidal load is applied on SABER and MATHCAD softwares to find more accurate results. However, the voltage gain, which is $Gain = |\frac{v_2}{v_1}|$, of this topology is determined. In Figure 3.8 is shown that the voltage gain of the PT system versus the various of different switching frequency f_{sw}. The switching frequency will be equal to the resonant frequency in 10k Hz where the voltage gain arrives to the peak value. The reason behind the peak value of voltage gain at 10k Hz is the reactance inductor canceled out by the reactance capacitor which means the drop voltage on the resonant components are zero. Figure 3.8 shows the magnetic coupling coefficient effects on the voltage gain. In addition, It is obvious that the effects of resonant compensated capacitors from Figure 3.8 where the input voltage to the transformer is approximately equal to the output voltage at the resonant frequency with different magnetic coupling coefficient values. The compensation capacitors at the resonant frequency can affect by adjusting the phase angle difference between the input and output voltage that caused by the inductors as shown in Figure 3.10. However, the output DC voltage of the rectifier, which is on the second side of the PT system circuit, is affected by the compensated capacitors. Figure 3.9 shows both the output DC voltage while applying the series resonant compensation capacitors and without applying the compensated capacitors on the PT system versus the varies magnetic coupling coefficient k values. It is noticeable that the DC voltage of the rectifier increases by increasing the magnetic coupling coefficient k value when the compensated capacitors are not applied on the PT system. However, the output DC voltage of the rectifier with applying the compensated capacitors is almost constant when the magnetic coupling coefficient values is changed. Moreover, the output DC voltage starts increasing more when k is high around $k = 0.95$. The increasing voltage happens because L_{s1} and L_{s2} are very small and almost like a short circuit, where $L_{s1} = (1-k)L_1$ and $L_{s2} = (1-k)L_2$, while the compensated

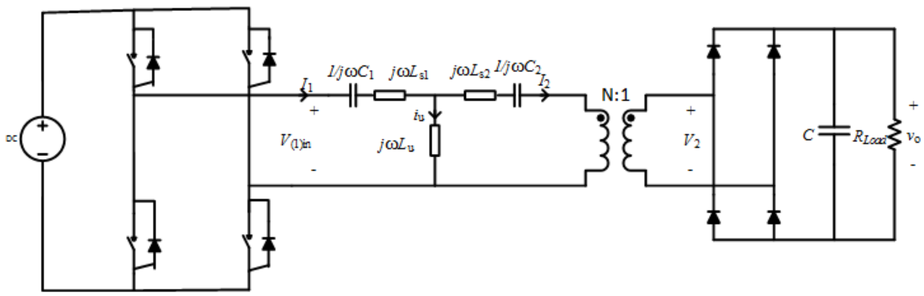

Figure 3.7 The power transfer between non-sinusoidal source and load with compensation capacitors.

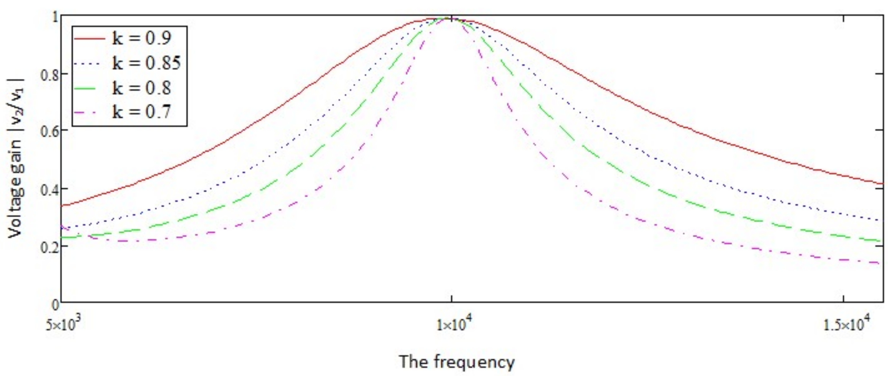

Figure 3.8 The voltage gain of power transfer between non-sinusoidal source and load versus different switching frequency.

capacitors begin by having very large values based on the result of the equation . Also, the contactless transformer with very high k acts as a transformer that transfers almost the same amount of power from the primary to the secondary side.

Hence, the only losses in this circuit is the losses on the resistance. While the resistance is very small, then the power loss is small. So, the power transfer between a non-sinusoidal source and a non-sinusoidal load efficiency improved to be around 99%.

However, to determine the efficiency of the PT between a non-sinusoidal source and a non-sinusoidal load with compensated capacitors, the output and input power of this converter will be calculated by using AC analytical technique. Figure 3.11 shows the PT circuit by using ac analytical technique.

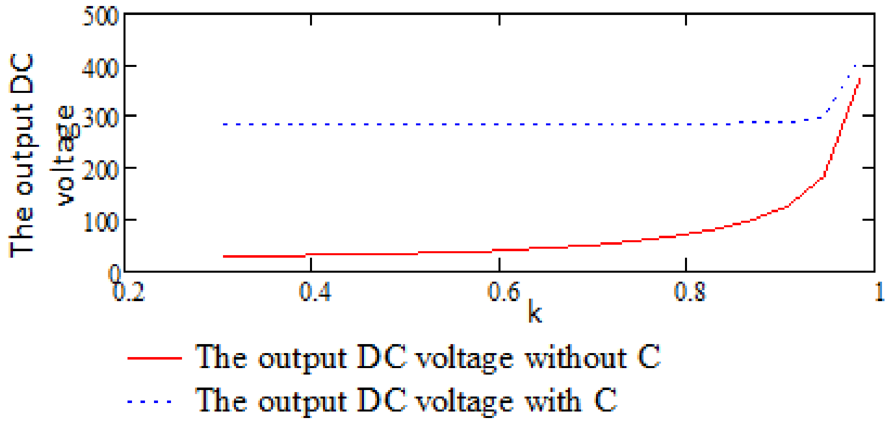

Figure 3.9 The output DC voltage on the R_L with and without compensated capacitors verses the magnetic coupling values

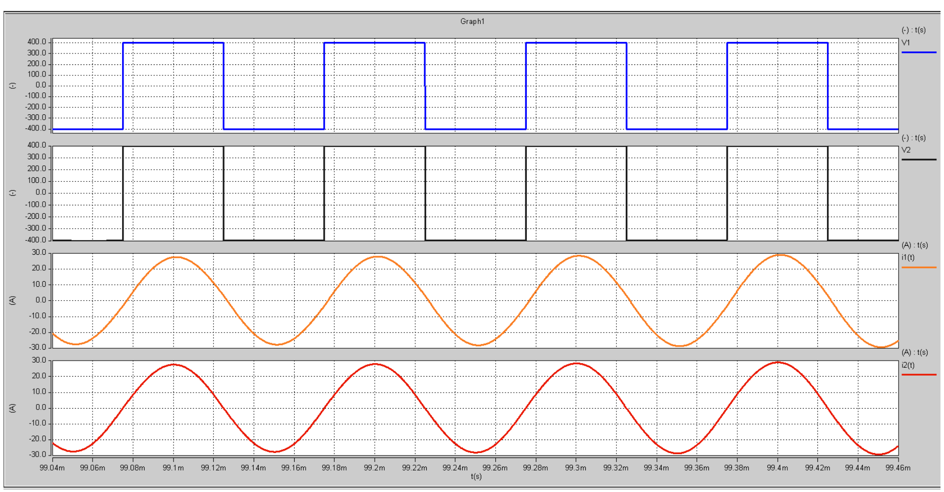

Figure 3.10 Shows the input and output voltages of the contactless tranformer and the both currents of the coils.

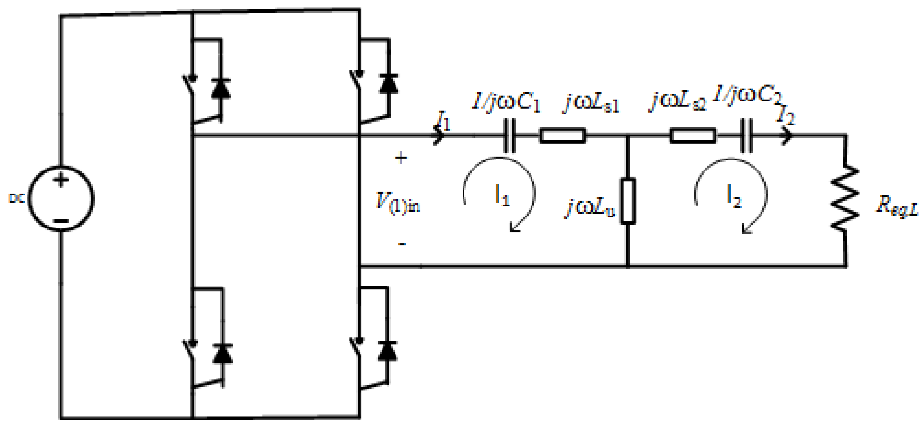

Figure 3.11 The power transfer between non-sinusoidal source and load with equivalent load resistance.

$$I_2 = \frac{V_{in(1)}}{\frac{(Z_{s1}+Z_\mu)(Z_{s2}+Z_\mu+R_{eq,L})}{Z_\mu} - Z_\mu} \tag{3.15}$$

So, the relationship between primary current I_1 and secondary current I_2 is show next

$$I_1 = \frac{Z_{s2}+Z_\mu+R_{eq,L}}{Z_\mu} I_2 \tag{3.16}$$

Hence, the input average power can be determined by returning $V_{in(1)}$ and I_1 from phasor domain to time domain after that taking the average value as following

$$i_1(t) = |I_1| sin(\omega t + arg(I_1)) \tag{3.17}$$

$$v_{in(1)}(t) = |V_{in(1)}| sin(\omega t + arg(V_{in(1)}) \tag{3.18}$$

$$P_{in}(k) = \frac{1}{T}\int_0^T i_1(t) v_{in(1)}(t) dt \tag{3.19}$$

$$P_{in}(k) = \frac{|I_1||V_{in(1)}|}{2} cos(arg(V_{in(1)}) - arg(I_1)) \tag{3.20}$$

The average output power $P_{out}(k)$ can be found by using the secondary current $i_2(t)$ where $i_2(t)$ is shown next

$$i_2(t) = |I_2| sin(\omega t + arg(I_2)) \tag{3.21}$$

$$P_{out}(k) = \frac{1}{T}\int_0^T i_2(t)^2 R_{eq,L} dt \tag{3.22}$$

$$P_{out}(k) = I_{2RMS}^{2} R_{eq,L} \tag{3.23}$$

where the RMS of sine wave current is

$$I_{2RMS} = \frac{I_{2Max}}{\sqrt{2}} \tag{3.24}$$

Hence, the output average power of power transfer converter with resonant compensation capacitors is

$$P_{out}(k) = (\frac{I_{2Max}}{\sqrt{2}})^{2} R_{eq,L} \tag{3.25}$$

So, the efficiency formula of the PT converter is

$$\eta(k) = \frac{P_{out}(k)}{P_{in}(k)} \tag{3.26}$$

3.3 Conclusion and Discussion

In the end of this chapter, the resonant compensation capacitors were applied to the power transfer between a non-sinusoidal source and a non-sinusoidal load model. The reason behind applying the compensated capacitors is to improve the efficiency of PT converter. The compensated capacitors, which are C_1 and C_2, are applied as series with the leakage inductances L_{s1} and L_{s2}, respectively. The main feature of the power transfer converter model that is how selecting the compensated capacitors values. The compensated capacitors values are selected by the formula that depends on the leakage inductances L_{s1} and L_{s2} where the leakage inductances are a primary and secondary self-inductance multiplied by $(1-k)$ where k is the magnetic coupling coefficient. This way of the capacitor calculating is helpful to give a good performance to the power transfer converter by including the leakage inductance value. However, the effects of the compensation capacitors on the power transfer converter efficiency are obvious for improving the efficiency. So, selecting the compensated capacitors values at the resonant frequency f_o, when f_o is equal to switching frequency f_{sw}, gives the best efficiency of power transfer converter.

CHAPTER 4

APPLICATIONS

Wind energy is one of the renewable energies that can reduce climate change since wind generation has zero emissions and low environmental effects [13]. Moreover, USA vision for 2030 is an increase in electrical power energy consumption from wind energy by 20% of electric energy network [19]. Hence, the power transfer between a non-sinusoidal source and a non-sinusoidal load will be applied on wind turbine.

This chapter will cover the resonant compensation topology of PT system. In the second section, the wind turbine on offshore will be considered for applying PT system. In the last section, the result of applying the power transfer system to wind renewable energy are discussed.

4.1 Capacitor Topology of Power Transfer System

Several different compensated capacitor topology can be applied to the power transfer system [20]. Figure 4.1 shows four different topologies for applying compensation capacitor to the PT system. First two topologies have connected a compensation capacitor in parallel to transmitter coil and the receiver coil is connected to a series capacitor or a parallel capacitor. This model, which has a parallel capacitor is connected to the transmitter coil, requires an additional inductor connected in series between the inverter and resonant circuit [9, 21]. The series additional inductor can be used to regulate the current of inverter that follows into the parallel resonant network [20]. Moreover, the additional inductor can achieve soft switching of the full-bridge inverter [9]. This type of topologies is beneficial for power transfer system that has various receivers and power distribution networks where a high circulating current is controlled in a power track [7, 9, 21, 22]. For a system that has a single receiver the series compensated capacitor connected to transmitter coil can avoid the power losses in the additional inductor [21]. Any inductor has the winding resistance and capacitance that dissipates both power and energy storage and dissipated of an inductor can be

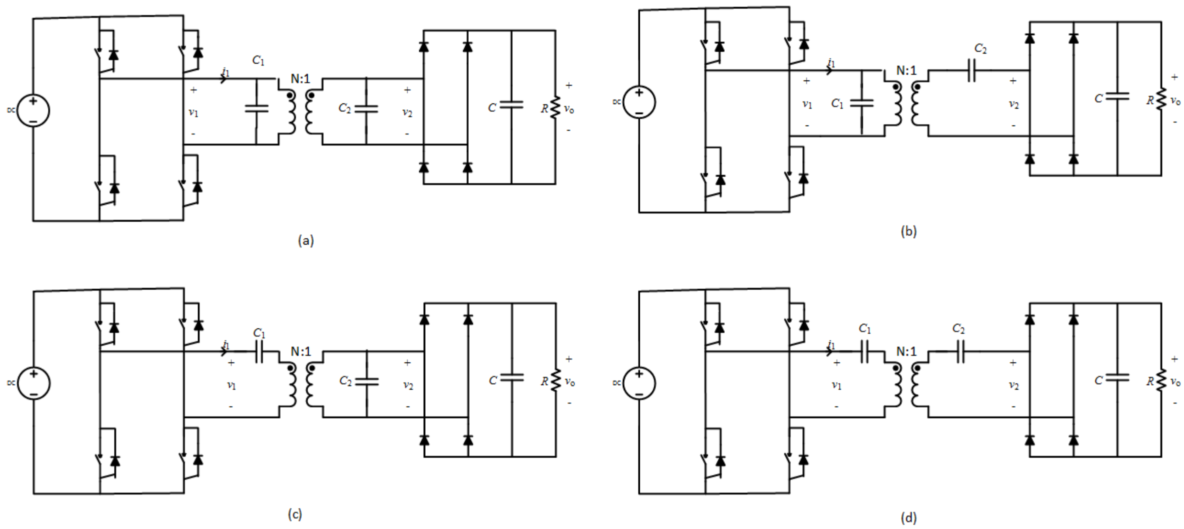

Figure 4.1 The possible topologies of power transfer system for single resonant primary capacitor and single resonant secondary capacitor: (a) parallel-parallel resonant compensated capacitors. (b) parallel-series resonant compensated capacitors. (c) series-parallel resonant compensated capacitors. (d) series-series resonant compensated capacitors.

calculated as following [15].

$$\varpi = \frac{1}{2}Li^2 \tag{4.1}$$

where ϖ is the energy storage of inductor.

However, in order to find better efficiency through less power losses and less components, the resonant compensated capacitor will be applied in series to the transmitter coil.

The other two topologies can be applied to the PT system that are a series or parallel compensated capacitor connected to receiver coil while the transmitter coil is connected with a series compensated capacitor. These models are shown in (c)and (d) of Figure 4.1. The parallel compensation of the receiver coil model has the advantage of reducing the insulation requirements because the voltage across resonant receiver network is low [9]. This model is used in medical implants for low power. However, the power losses in this model is higher than series compensation receiver model where the additional reactive current happens in the resonant circuit at light condition [23]. Additionally, a series-parallel compensated model is dependent on two factors which are a load condition and a magnetic coupling of the coil, where the resonant capacitors must be selected as explained in [21].

$$C_1 = \frac{1}{\omega_o^2 L_1 (1-k^2)} \tag{4.2}$$

$$C_2 = \frac{1}{\omega_o^2 L_2} \tag{4.3}$$

C_1 is depended on the coils position. Then it should be selected based on the magnetic coupling of inductors. So, if there is any misaligned in coils places of the PT system, the efficiency will be decreased because of additional conduction losses. Also, this will increase losses in the converter due to increasing the losses current in the switching [21]. Hence, the best resonant compensated topology for power transfer system is series-series compensation. This method is independently model where compensated capacitors will be selected independent from load condition and the air gap distance. the primary and secondary compensated capacitors must be chosen as shown below

$$C_1 = \frac{1}{\omega_o^2 L_1} \tag{4.4}$$

$$C_2 = \frac{1}{\omega_o^2 L_2} \tag{4.5}$$

4.2 Wind Turbine

The use of wind energy to generate electricity power is seeing an increase in implementation on a global scale [3, 13]. The main goal of many investors and manufacturers is to generate more power with reduced visual effects and losses, and the offshore windfarms offer a solution alongside other desirable features [4, 13]. Said features will be explained below [13]. First, the wind turbines are located at a distance far from the shore so the generated power is higher and more constant. Additionally, High Voltage Direct Current (HVDC) is very appropriate technology for a long distance because it can minimize the losses in the transmission line. Furthermore, the velocity of wind is higher and more constant, so the output energy of the generation system is higher [13]. The different topologies of offshore wind farms have been investigated [12, 13]. A brief overview of different offshore wind turbines and farms identifies the cluster method as having two types of

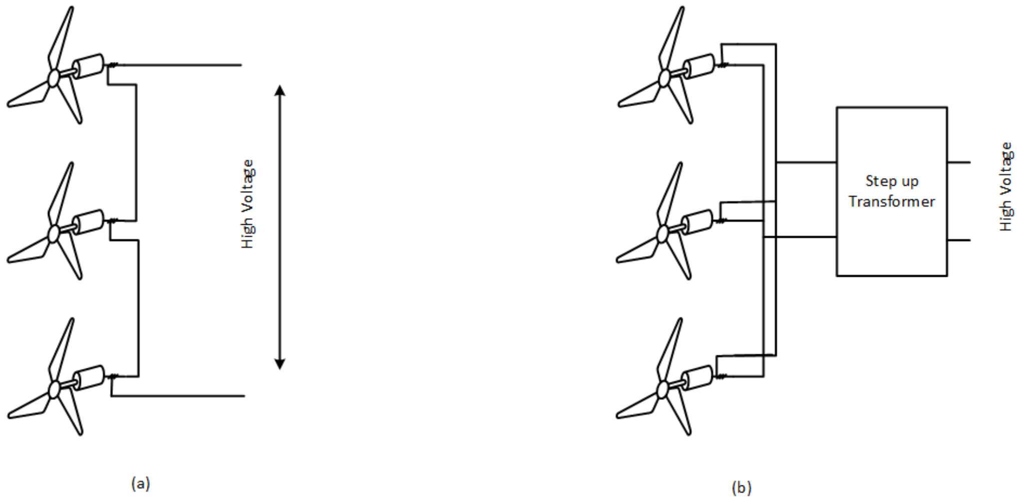

Figure 4.2 Different connected topology of wind turbines in farm: (a) The wind turbines are connected in series. (b)The wind turbines are connected in parallel.

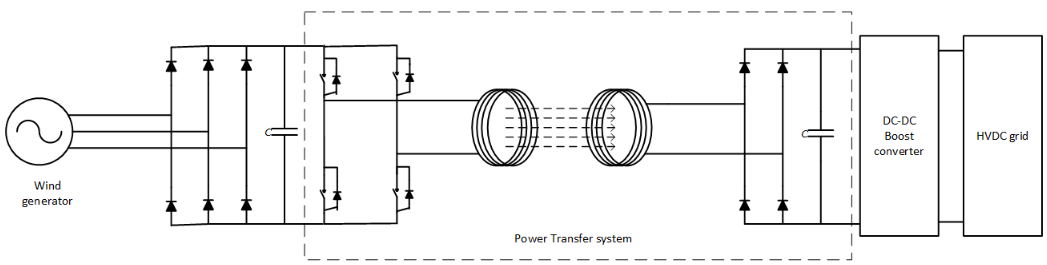

Figure 4.3 The power transfer between non-sinusoidal source and load in the wind energy network.

clusters: A series connection of parallel connected turbines which are called ac clusters, and the dc clusters which are a parallel connection of series connected turbines. However, there are two types of turbine connections in parks with no clusters, series wind turbine connections or parallel wind turbine connections. In Figure 4.2 it shows when the wind turbines are connected in series in part (a), in part (b) it shows when the wind turbines are connected in parallel. The series connection of wind turbines can achieve a high voltage level without needing to use step-up transformer station. Thus, there are no losses in the transformer. Furthermore, it will reduce the investment cost of platform. On the other hand, the parallel connections of wind turbines have a high reliability but the losses of offshore grid are high [13].

In this thesis, a permanent magnet synchronous machine (PMSM) is considered as generator due to its numerous advantages. There are some advantages of PMSM in wind energy according to [13, 24]: It has lower maintenance cost because it does not have gearboxes. Moreover, its efficiency is high over a large power range. Another important feature of PMSM is that the rotor does not have significant losses in itself. However, the power transfer between a non-sinusoidal source and a non-sinusoidal load across inductive network will be applied to wind turbine energy in the next section.

4.2.1 The power transfer between non-sinusoidal source and load applied to wind turbine

In order to transfer electric power wirelessly from a wind turbine to HVDC grid, the PT system is applied to wind turbine energy. Figure 4.3 shows the power transfer between a non-sinusoidal source and a non-sinusoidal load is applied to wind power network. The three phase full bridge rectifier converts ac voltage from PMSM generator to dc voltage in order to apply it into the PT system. After that, the dc voltage goes to the full bridge inverter for converting dc voltage to alternative square voltage with high frequency which is 10kHz. This alternative square voltage transfer across a primary winding to a secondary (receiver) winding through air-gap. After the square voltage received, the rectifier, which is in the secondary side, converts the square voltage to dc voltage. Then, dc-dc converter raises the voltage to the desired voltage for HVDC transmission line. In order to model the whole system, Figure 4.4 shows the power transfer system with wind turbine in details.

The values of circuit parameters are shown in Table 4.1. The line to line RMS voltage $V_{l-l(rms)}$ of the wind turbine generator is 427V with frequency value is 60Hz. However, the output voltage of full-bridge rectifier can be calculated as following

$$V_{dc(3\Phi)} = \frac{1}{T} \int_{\frac{\pi}{3}}^{\frac{2\pi}{3}} V_{l-l(Max)} \sin(\theta) d\theta \tag{4.6}$$

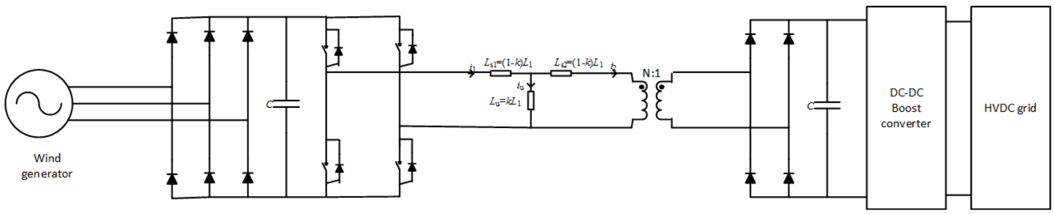

Figure 4.4 The model of power transfer between non-sinusoidal source and load in the wind energy network.

where $V_{dc(3\phi)}$ is the average output voltage of full-bridge rectifier. $V_{l-l(Max)}$ is the maximum line to line voltage value of the source.

$$V_{dc(3\phi)} = \frac{6}{2\pi} \int_{\frac{\pi}{3}}^{\frac{2\pi}{3}} \sqrt{2} V_{l-l(rms)} \sin(\theta) d\theta \tag{4.7}$$

$$V_{dc(3\phi)} = \frac{3\sqrt{2}}{\pi} V_{l-l(rms)} \tag{4.8}$$

Equation 4.8 can be used to determine the average output voltage of three-phase full bridge rectifier. Moreover, the output dc voltage of the rectifier can be reached to maximum voltage $V_{l-l(Max)}$ by using high capacitance. The capacitance filter C_r can work as regulator or voltage sink where it can remove the ripple of output voltage. where, the ripple voltage can be calculated as

$$V_{r(pp)} = \frac{V_{l-l(Max)}}{f_r R C_r} \tag{4.9}$$

The ripple frequency f_r is six times the input frequency [17]. The average output voltage value can be selected base on the capacitance filter

$$V_{dc(3\phi)} = V_{l-l(Max)} - V_{r(pp)} \tag{4.10}$$

The capacitance filter can be selected from the following formula [17]

$$C_r = \frac{V_{l-l(Max)}}{-2 f_r R (V_{dc(3\phi)} - V_{l-l(Max)})} \tag{4.11}$$

Table 4.1 Parameters value of the power transfer system with wind turbine.

Parameter	Variable	Value
Output power	P_{out}	$\leq$100k W
RMS Line-Line voltage	$V_{l-l(rms)}$	427V
RMS single-phase voltage	$V_{1\phi(rms)}$	246V
Input DC voltage	V_1	600 V
Output DC voltage	V_{out}	$\leq$600 V
Switching frequency	f_{sw}	10k Hz
Primary self-inductance	L_1	0.5m H
Secondary self-inductance	L_2	0.5m H

Thus, the output voltage of three-phase full-bridge rectifier is the DC voltage which has the value of maximum line to line voltage source with no ripple if the output capacitor is very high. Then,the output dc voltage can work as a DC voltage source for the PT system with 600 dc voltage.

The dc input voltage is applied to full-bridge inverter with PWM technique in order to convert the dc voltage to alternative square voltage. The switching frequency f_{sw} that is applied to the inverter is 10kHz. The square wave voltage ,which is out of inverter, has an amplitude of the dc voltage input with high frequency 10kHz in order to transfer it from a primary coil to a secondary coil. The model of coils of the primary and secondary sides are shown in Figure 4.4. This model is explained in detail in the previous chapters. Figure 4.5 shows the input and output voltages and current of cantactless transformer with high power level with different coefficient magnetic coupling values. Part (a)shows the voltages and currents when $k = 0.99$ with high level of power 100kW while part (b)is the input and output voltages and currents when $k = 0.97$.

It is noticeable that the secondary voltage is affected by the distance between the primary and secondary coils. It means the secondary voltage is reduced when the coefficient magnetic coupling value decreases. Figure 4.6 shows the voltage gain $\frac{V_{out}}{V_{in}}$ of the PT system when it is applied to transfer power of wind turbine generator to the boost dc-dc converter. The voltage gain curve presents the relation between magnetic coupling coefficient value k and output voltage in the secondary side of the PT system. The relation is directly proportional between k and the output voltage where with high value of k ,which is $k \approx 1$, the voltage gain has approximate unity value.

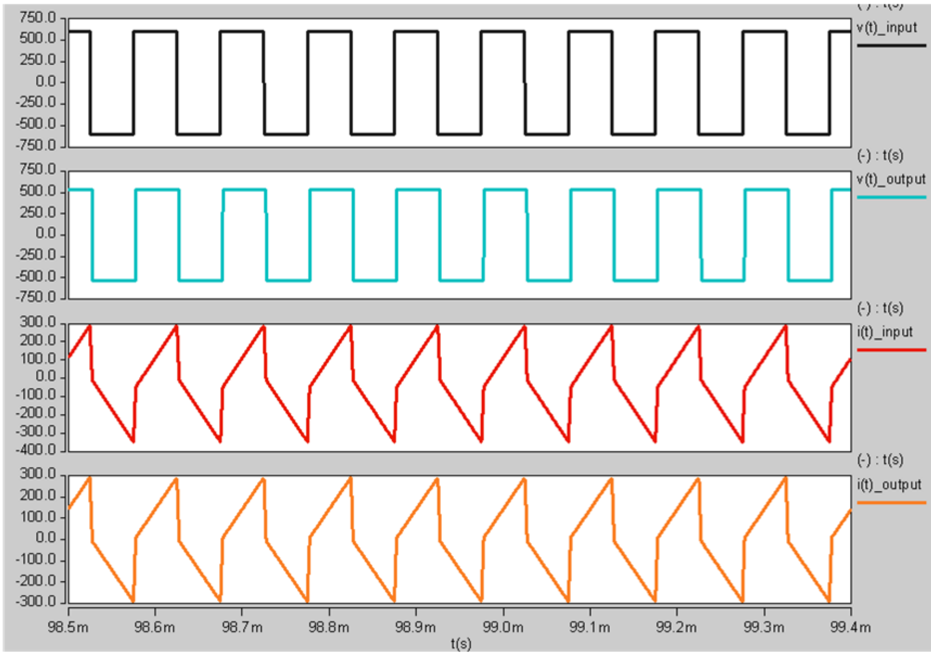

(a)

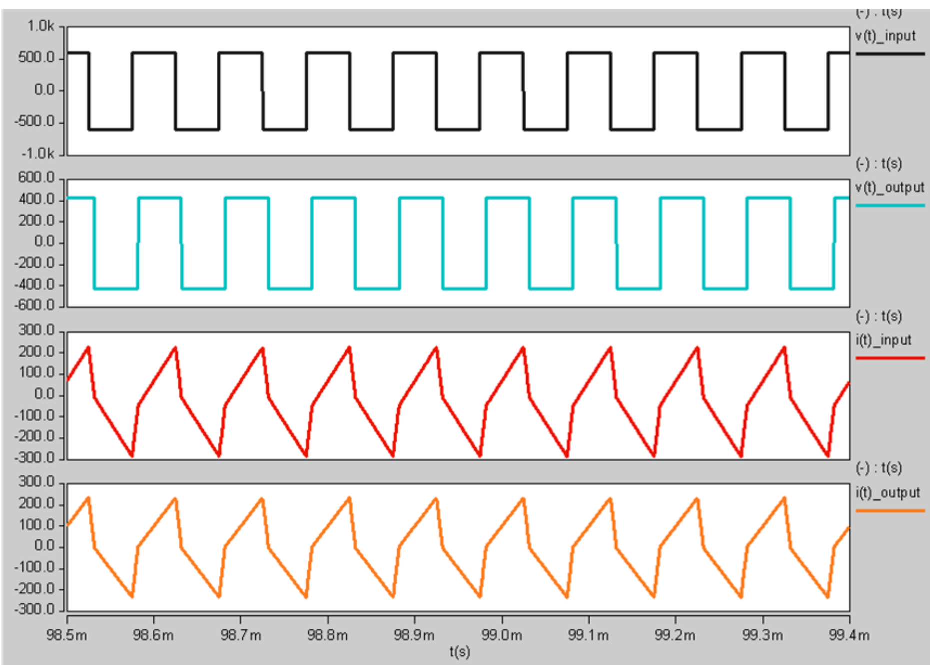

(b)

Figure 4.5 The waveforms characteristics of power transfer system with input voltage 600V: (a) The input and output voltages and currents of power transfer system with $k = 0.99$. (b)The input and output voltages and currents of power transfer system with $k = 0.97$

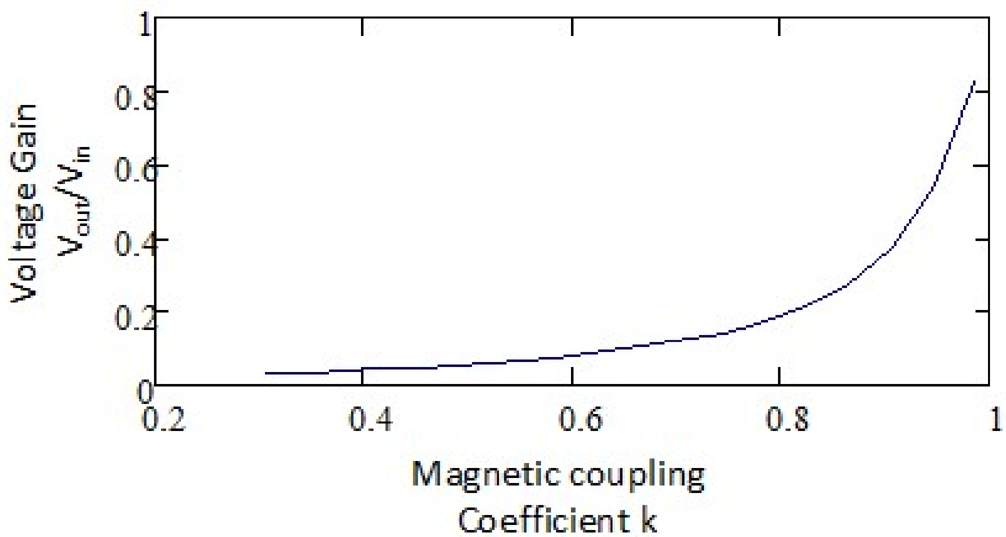

Figure 4.6 The voltage gain $\frac{V_{out}}{V_{in}}$ of the power transfer system at wind electric energy network with applying varies magnetic coupling coefficient k.

That means the output voltage is equal to input voltage also, the PT system will act as galvanic isolation.

4.2.1.1 The efficiency of power transfer system at wind energy system

In order to determine the efficiency of power transfer system between non-sinusoidal source and load at wind electric energy system, the analytical calculations are made it in mathcad software to compare it with the simulation results of saber software. Figure 4.7 shows the efficiency curves of the PT system at wind electric energy system. These curves were calculated with varies magnetic coupling coefficient k that is between 0.305 and 0.985 in order to know the effects of k at the power transfer system efficiency.

Different magnetic coupling coefficient k can be taken arbitrarily to measure the efficiency of the converter and choose the lowest k with better efficiency. The magnetic coupling coefficient k that are chosen, are $k_1 = 0.99$, $k_2 = 0.98$, $k_3 = 0.97$, and $k_4 = 0.96$. So, the efficiency of each k values

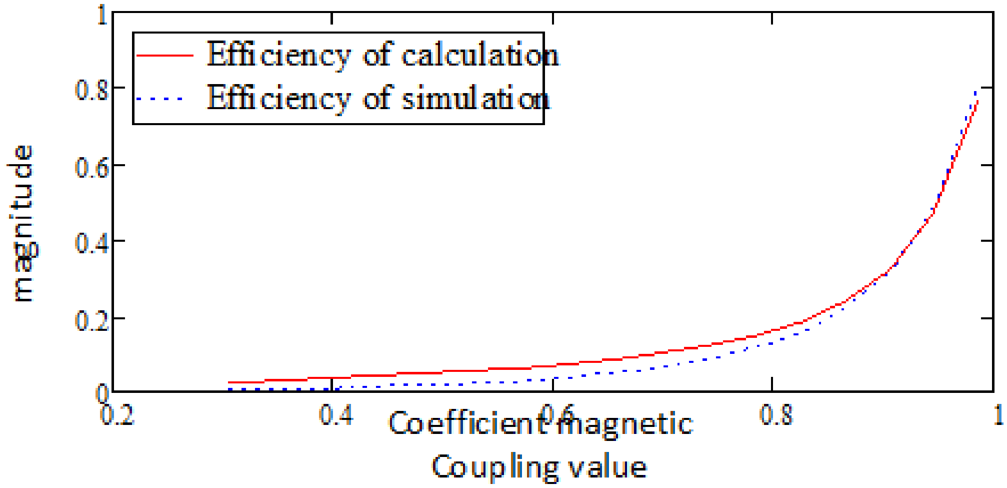

Figure 4.7 The efficiency curves of the power transfer system of wind electric energy network with applying varies magnetic coupling coefficient k where the solid curve is the efficiency that is calculated while the dot curve is the efficiency that taken by simulation.

,which were chosen, are as following

$$\eta(k_1) = \frac{P_{out}(k_1)}{P_{in}(k_1)} = 82.8\% \tag{4.12}$$

$$\eta(k_2) = \frac{P_{out}(k_2)}{P_{in}(k_2)} = 71.5\% \tag{4.13}$$

$$\eta(k_3) = \frac{P_{out}(k_3)}{P_{in}(k_3)} = 62.7\% \tag{4.14}$$

$$\eta(k_4) = \frac{P_{out}(k_4)}{P_{in}(k_4)} = 55.6\% \tag{4.15}$$

Hence, the PT system efficiency is decreased by increasing the air gap distance between the two contactless transformer sides. So, the lowest magnetic coupling coefficient k with efficiency that higher than 50% is $k = 0.96$ for this particular circuit.

4.2.1.2 Conclusion and Discussion

This model of wireless power transfer system which called the power transfer system between a non-sinusoidal source and a non-sinusoidal load can be applied for high level of power with same result to medium and low level of power. The PT system is applied to wind electric energy system

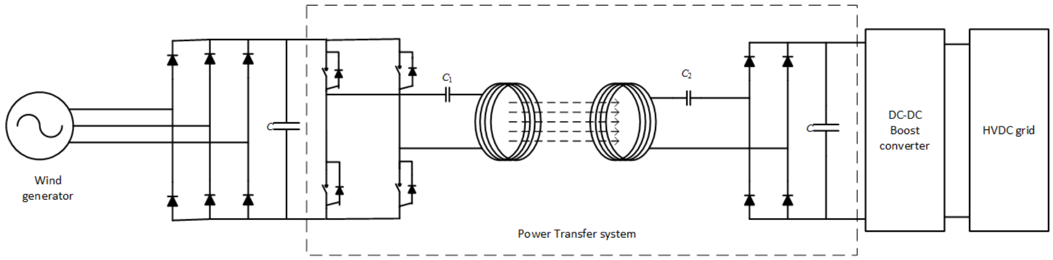

Figure 4.8 The power transfer between non-sinusoidal source and load with resonant compensation circuit is in the wind energy network.

with high power level is $P = 100k$ W. This model has many advantages that can be considered for application in actual field of high power level. One of advantages of the PT system is to transfer the power without using cables which will reduce the cable cost of network system. Also, the PT system can act as galvanic isolation which is important to protect the generators for insulation purposes. However, the efficiency of power transfer system between a non-sinusoidal source and a non-sinusoidal load model can be improved by applying resonant compensated impedances network. In the next section, the power transfer system between non-sinusoidal source and load with resonant compensation capacitors is applied to wind electric energy network.

4.2.2 Series-Series resonant compensated capacitors applied to power transfer system at wind electric energy system

In order to improve the efficiency of power transfer system between a non-sinusoidal source and a non-sinusoidal load in the wind electric energy system, the compensated capacitors are applied to the PT system. Figure 4.8 shows the power transfer system that is placed in the wind electric energy system with series-series resonant compensated capacitors. This method of applying compensation capacitors is useful to reduce the effects of leakage inductances in the PT system.

The compensation capacitors can be determined based on this formula 3.2.

$$C_1(k) = C_2(k) = \frac{1}{\omega_s^2 L_{s1}(k)} \tag{4.16}$$

where $\omega_s = 4\pi^2 f_s$ is the resonant angular speed. One of the main advantages to apply a high frequency f_s as a resonant frequency to the PT system is decreasing the components size of the

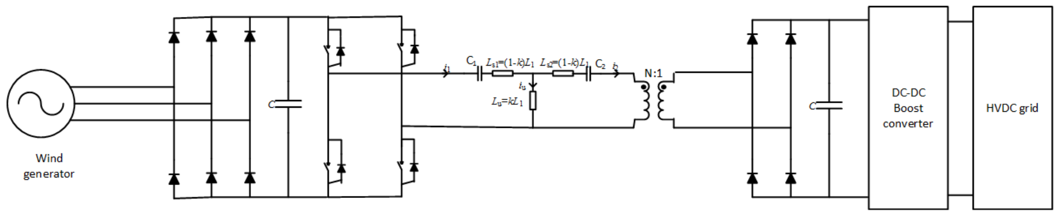

Figure 4.9 The model of power transfer between non-sinusoidal source and load with series-series resonant compensated capacitors is in the wind energy network.

system. For instance, the inductors and capacitors are calculated at $k = 0.97$ where $L_{s1} = 15\mu$H as shown below

$$C_1(0.97) = \frac{1}{\omega_s^2 15\mu} \tag{4.17}$$

$$C_1(0.97) = 16.89\mu F \tag{4.18}$$

The power transfer system with resonant compensated capacitors which is placed in the wind electric energy system is shown in Figure 4.9. It is shown that the topology of contactless transformer with series-series resonant compensated capacitors. The input and output voltage and current characteristic waveforms of this topology in wind electric energy system are shown in Figure 4.10. Part (a) is shown the characteristic waveforms of voltages and currents when the magnetic coupling coefficient k is equal to 0.99 while part (b) is displayed the input and output voltages and currents when the distance between primary and secondary coils is increased with $k = 0.97$. It is clearly noticeable that the primary and secondary currents of the coils with series-series compensation capacitors are sinusoidal-waveforms. This phenomenon of changing the current waveforms from non-sinusoidal to sinusoidal shape happens because of the resonant compensation capacitors which filters the harmonics of the input power. Moreover, It reduces the losses by the fact that the capacitor and inductor cancel their drop voltages out if they have same resonant frequency.

Hence, the voltage gain of the power transfer system in the wind electric energy system is improved as shown in Figure 4.11. The effects of the resonant circuit on the PT system at wind electric energy system are obvious through the voltage gain where it is applied with various mag-

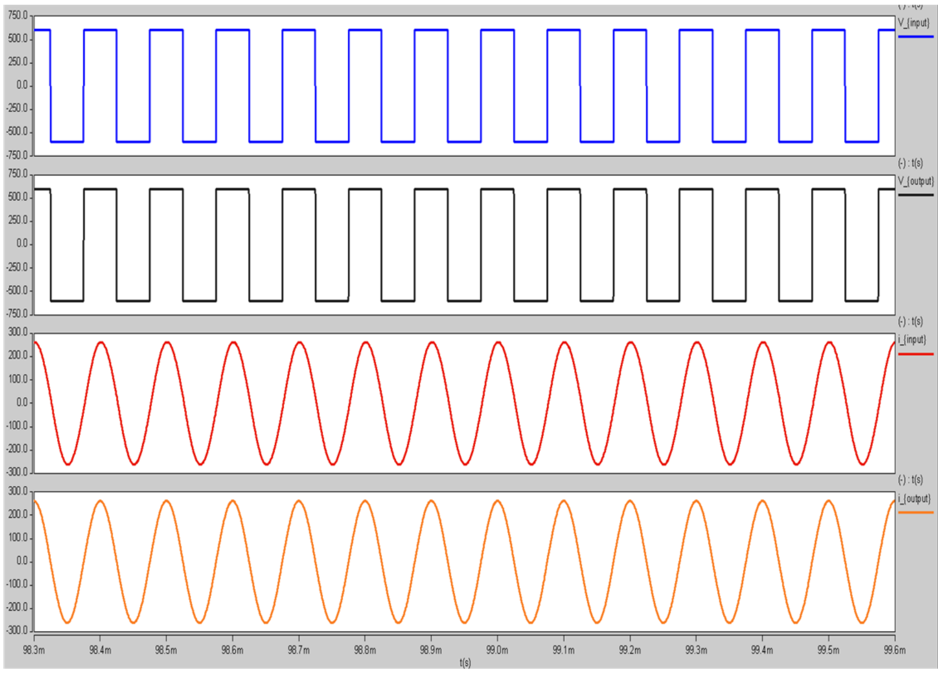

(a)

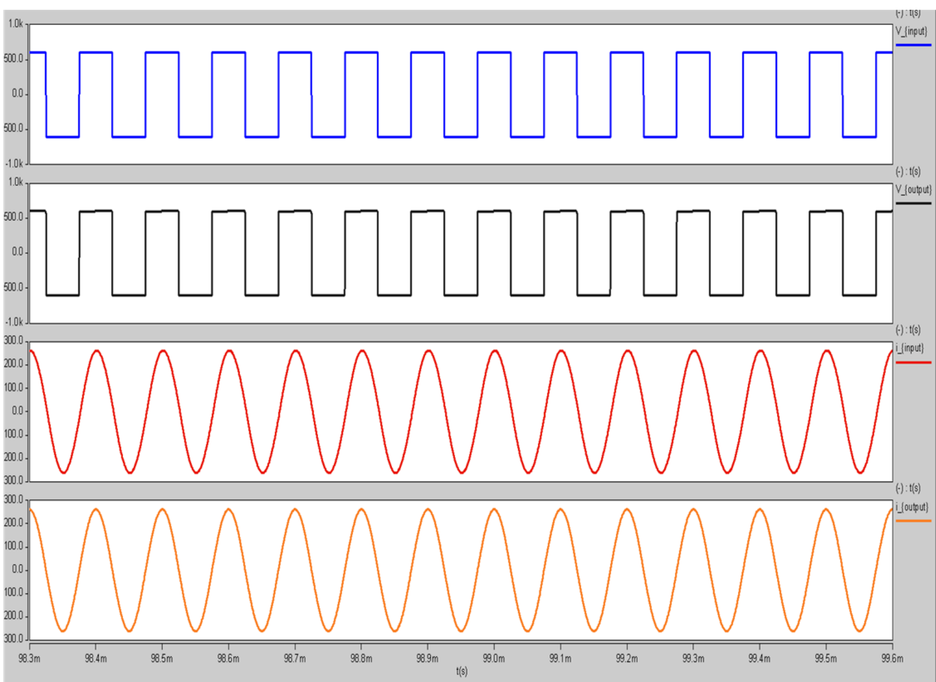

(b)

Figure 4.10 The waveforms characteristics of power transfer system when the resonant compensation capacitors are applied with input voltage 600V: (a) The input and output voltages and currents of power transfer system with $k = 0.99$. (b)The input and output voltages and currents of power transfer system with $k = 0.97$

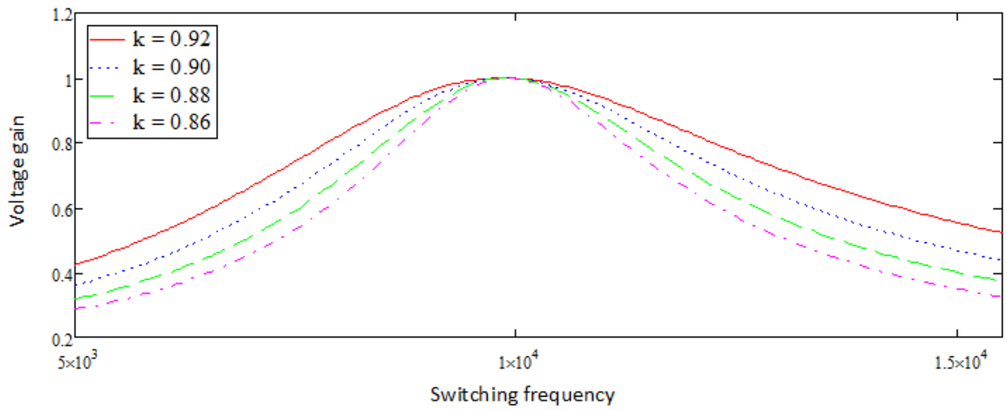

Figure 4.11 The voltage gain of the power transfer system with series-series resonant compensated capacitors versus the switching frequency with several different magnetic coupling coefficients k.

netic coupling coefficient values.

Therefore, the magnitude value of the voltage gain with varies magnetic coupling coefficient values are approximately one when the switching frequency f_{sw} is equal to the resonant frequency $f_o = 10k$Hz. On the other hand, the magnitude value of the voltage gain is decreased when the switching frequency is smaller or greater than the resonant frequency. When the switching frequency has value is more smaller or larger than the resonant frequency, the magnitude value of voltage gain begin more decreasing. It means the drop voltages on both coils and both capacitors are increased. Hence, the efficiency of the power transfer between a non-sinusoidal source and a non-sinusoidal load with series-series resonant compensation capacitors in wind electric energy system is satisfied when the resonant frequency is equal to switching frequency.

4.2.2.1 Conclusion and Discussion

In the end of this section, the power transfer between a non-sinusoidal source and a non-sinusoidal load with series-series resonant compensation capacitors are applied on the wind electric energy system by using two softwares. The softwares are SABER and MATHCAD. The main goal of applying compensation capacitors to the PT system is to improve the power transfer efficiency between non-sinusoidal source and load in order to transfer the power energy to HVDC transmission line grid. This topology with compensation capacitors has other advantages besides the improved efficiency which is achieved through previous section and chapters. Another important advantage is making the components size smaller. Then the system cost will be reduced due to decreasing the components size. Moreover, the drop voltages on the primary and secondary coils are canceled out by adding the resonant compensation capacitors at the same switch frequency. Furthermore, the efficiency of the power transfer system with series-series resonant compensation capacitors in the wind electric energy system is improved even if the magnetic coupling coefficient values vary when the switching frequency is equal to the resonant frequency.

CHAPTER 5

CONCLUSION AND OUTLOOK

The new model of transferring power between a non-sinusoidal source and a non-sinusoidal load across inductive network is presented in the previous chapters. The power transfer system model offers a satisfactory performance when applied to ranges of power level varying from medium to high amount. The results and conclusions drawn from the application of the PT system to a high amount of power are shown in the next section. A summary of the results of each chapter will be provided at their respective end. Only important results and conclusion are shown in the following. In the last section, some future work topics are suggested and considered in order to improve this model.

5.1 Results and Conclusions

In this thesis, the contact-less transformer model was introduced in the previous chapters. One of the main aims of introducing the fundamental analysis of the contact-less transformer is to show how it and the magnetic coupling coefficient has effects on the transformation results. Furthermore, the fundamental analysis yields that the reluctance of contact-less transformer is directly proportional to the air-gap distance between primary and secondary windings. Therefore, the main goal of this model is to make the reluctance value as a part of both inductors, then applied to be part of the power transfer system. This method helps improve the efficiency of the power transfer system via the resonant compensation capacitors' calculations. The compensated capacitors are calculated by including the whole primary and secondary self-inductances with reluctance value. Another advantage for including the reluctance value in the compensated capacitors calculations is that the components size is reduced which results in a higher cost efficiency. Hence, the power transfer system between a non-sinusoidal source and a non-sinusoidal load with series-series resonant compensation capacitors is utilized as an application in a high power field. This application is placed in the wind electric energy system. The performance of the power transfer system with resonant capacitors in the wind electric energy system accomplishes a high power efficiency. The results of this application are calculated and simulated by two different softwares. The MATHCAD software is used to apply the analytical calculations. On the other hand, the SABER software is used to simulate the PT system for different applications. Yet another advantage of using the PT system is the power transfer system does not have the complicated controllability which can help to spread this model to be adopted into a variety of fields. Another fact that should be mentioned is different inductors of the contactless transformer has different frequency value response. This fact is helpful to choose the appropriate inductor with matching the frequency value for experiments in order to have same results of the theory.

5.2 Future Research Topics

The main aim of the introducing this research is to build deep understanding and knowledge about the PT system. This information shows how the performance of transferring power efficiency can be improved. Also, it shows the possibility to apply the PT system in renewable energy with high amounts of power. According to the results found in this research, the foreseeable topics of future research areas are presented below:

- The power transfer system between non-sinusoidal source and load can be worked with multi receivers. The multi receivers of the PT system can be used for several purposes.
- Other research area that can be considered is improving the transferring power efficiency by applying a higher order of compensation. This topic has several advantages besides improving the efficiency that reduces the component sizes. It can also achieve the constant outputs current or voltage as well as the potential of achieving soft switching to the converter [25].

BIBLIOGRAPHY

BIBLIOGRAPHY

[1] J. Garnica, R. A. Chinga, and J. Lin, "Wireless power transmission: From far field to near field," *Proceedings of the IEEE*, vol. 101, no. 6, pp. 1321–1331, 2013.

[2] M. Pinuela, D. C. Yates, S. Lucyszyn, and P. D. Mitcheson, "Maximizing dc-to-load efficiency for inductive power transfer," *IEEE transactions on power electronics*, vol. 28, no. 5, pp. 2437–2447, 2013.

[3] G. A. Covic and J. T. Boys, "Inductive power transfer," *Proceedings of the IEEE*, vol. 101, no. 6, pp. 1276–1289, 2013.

[4] Y. Kaneko and S. Abe, "Technology trends of wireless power transfer systems for electric vehicle and plug-in hybrid electric vehicle," in *Power Electronics and Drive Systems (PEDS), 2013 IEEE 10th International Conference on*. IEEE, 2013, pp. 1009–1014.

[5] S. G. Cimen and B. Schmuelling, "Development of a modular inductive power transfer system with a reactive power correction for ev application," in *Power Electronics Conference (SPEC), IEEE Annual Southern*. IEEE, 2016, pp. 1–5.

[6] H. H. Wu, A. Gilchrist, K. Sealy, P. Israelsen, and J. Muhs, "A review on inductive charging for electric vehicles," in *Electric Machines & Drives Conference (IEMDC), 2011 IEEE International*. IEEE, 2011, pp. 143–147.

[7] F. Pellitteri, M. Caruso, V. Castiglia, A. Di Tommaso, R. Miceli, and L. Schirone, "An inductive charger for automotive applications," in *Industrial Electronics Society, IECON 2016-42nd Annual Conference of the IEEE*. IEEE, 2016, pp. 4482–4486.

[8] R. Bosshard and J. W. Kolar, "Multi-objective optimization of 50 kw/85 khz ipt system for public transport," *IEEE Journal of Emerging and Selected Topics in Power Electronics*, vol. 4, no. 4, pp. 1370–1382, 2016.

[9] R. Bosshard, "Multi-objective optimization of inductive power transfer systems for ev charging," Ph.D. dissertation, 2015.

[10] Y. J. Jang, Y. D. Ko, and S. Jeong, "Optimal design of the wireless charging electric vehicle," in *Electric Vehicle Conference (IEVC), 2012 IEEE International*. IEEE, 2012, pp. 1–5.

[11] Q. Chen, N. Liu, C. Hu, L. Wang, and J. Zhang, "Autonomous energy management strategy for solid-state transformer to integrate pv-assisted ev charging station participating in ancillary service," *IEEE Transactions on Industrial Informatics*, vol. 13, no. 1, pp. 258–269, 2017.

[12] N. Holtsmark, H. J. Bahirat, M. Molinas, B. A. Mork, and H. K. Hoidalen, "An all-dc offshore wind farm with series-connected turbines: An alternative to the classical parallel ac model?" *IEEE Transactions on industrial Electronics*, vol. 60, no. 6, pp. 2420–2428, 2013.

[13] A. Garcés and M. Molinas, "A study of efficiency in a reduced matrix converter for offshore wind farms," *IEEE Transactions on Industrial Electronics*, vol. 59, no. 1, pp. 184–193, 2012.

[14] F. Musavi and W. Eberle, "Overview of wireless power transfer technologies for electric vehicle battery charging," *IET Power Electronics*, vol. 7, no. 1, pp. 60–66, 2014.

[15] C. K. Alexander and M. no Sadiku, "Electric circuits," *Transformation*, vol. 135, pp. 4–5, 2000.

[16] M. Staff, "Magnetic circuits and transformers," *Wilev, NY*, 1943.

[17] M. H. Rashid, *Power electronics handbook: devices, circuits and applications*. Academic press, 2010.

[18] R. L. Steigerwald, "A comparison of half-bridge resonant converter topologies," *IEEE transactions on Power Electronics*, vol. 3, no. 2, pp. 174–182, 1988.

[19] E. Veilleux and P. W. Lehn, "Interconnection of direct-drive wind turbines using a series-connected dc grid," *IEEE Transactions on Sustainable Energy*, vol. 5, no. 1, pp. 139–147, 2014.

[20] C.-S. Wang, O. H. Stielau, and G. A. Covic, "Design considerations for a contactless electric vehicle battery charger," *IEEE Transactions on industrial electronics*, vol. 52, no. 5, pp. 1308–1314, 2005.

[21] R. Bosshard, J. W. Kolar, J. Mühlethaler, I. Stevanović, B. Wunsch, and F. Canales, "Modeling and \eta $-\backslash alpha$-pareto optimization of inductive power transfer coils for electric vehicles," *IEEE Journal of Emerging and Selected Topics in Power Electronics*, vol. 3, no. 1, pp. 50–64, 2015.

[22] K. W. Klontz, D. M. Divan, D. W. Novotny, and R. D. Lorenz, "Contactless power delivery system for mining applications," *IEEE Transactions on Industry Applications*, vol. 31, no. 1, pp. 27–35, 1995.

[23] O. Knecht and J. W. Kolar, "Impact of transcutaneous energy transfer on the electric field and specific absorption rate in the human tissue," in *Industrial Electronics Society, IECON 2015-41st Annual Conference of the IEEE*. IEEE, 2015, pp. 004 977–004 983.

[24] M. Fu, H. Yin, X. Zhu, and C. Ma, "Analysis and tracking of optimal load in wireless power transfer systems," *IEEE Transactions on Power Electronics*, vol. 30, no. 7, pp. 3952–3963, 2015.

[25] X. Qu, Y. Jing, H. Han, S.-C. Wong, and K. T. Chi, "Higher order compensation for inductive-power-transfer converters with constant-voltage or constant-current output combating transformer parameter constraints," *IEEE Transactions on Power Electronics*, vol. 32, no. 1, pp. 394–405, 2017.